Acta Pharmaceutica Sinica B 2026;16(2):930−947

Chinese Pharmaceutical Association
Institute of Materia Medica, Chinese Academy of Medical Sciences

Acta Pharmaceutica Sinica B

www.elsevier.com/locate/apsb
www.sciencedirect.com

ORIGINAL ARTICLE

Cold exposure-induced β-hydroxybutyrate promotes brown fat mitochondrial lipid droplet contact to ameliorate fatty dysfunction and hepatic steatosis

Yuanyuan Yu[a], Na An[a], Yi Chen[a], Ming Tong[a], Shuyu Liu[a], Yanrong Li[a], Hongbo Dong[a], Yanxi Li[a], Min Feng[a], Linhe Liu[a], Shifeng Cao[a], Huan Chen[a], Yixiu Zhao[a], Zhimin Du[b,c], Xin Zhao[a,*], Baofeng Yang[a,d,*], Yan Zhang[a,*]

[a]*State Key Laboratory of Frigid Zone Cardiovascular Diseases (SKLFZCD), Department of Pharmacology (State Key Labratoray-Province Key Laboratories of Biomedicine-Pharmaceutics of China, Key Laboratory of Cardiovascular Research, Ministry of Education), College of Pharmacy, Harbin Medical University, Harbin 150081, China*
[b]*Institute of Clinical Pharmacology, The Second Affiliated Hospital of Harbin Medical University (National Key Laboratory of Frigid Cardiovascular Disease), Harbin 150081, China*
[c]*State Key Laboratory of Quality Research in Chinese Medicines, Macau University of Science and Technology, Macau 999078, China*
[d]*Research Unit of Noninfectious Chronic Diseases in Frigid Zone (2019RU070), Chinese Academy of Medical Sciences, Harbin 150081, China*

Received 7 April 2025; received in revised form 5 June 2025; accepted 15 June 2025

KEY WORDS

β-Hydroxybutyrate;
Mitochondrial lipid droplet contact;
RAB10−PLIN5 complex;
Cold exposure;
HADHA;

Abstract Cold exposure activates brown adipose tissue (BAT), to alleviate metabolic disorders. However, the mechanisms underlying the regulation of mitochondrial lipid droplet contact (MLC) in BAT and their association with these benefits remain unclear. Here, we identify liver-derived β-hydroxybutyrate (BHB) as a key mediator in driving MLC formation in BAT. Mechanistically, BHB directly targets at the GLY-67 residue of RAB10, enhancing its interaction with PLIN5 to form the RAB10−PLIN5 complex, which facilitates MLC. This interaction was validated using SPIDER and biotin-labeled pull-down assays. Functionally, BHB treatment reduces lipotoxicity and improves metabolic health in diet-induced

*Corresponding authors.
E-mail addresses: zhangyan@ems.hrbmu.edu.cn (Yan Zhang), yangbf@ems.hrbmu.edu.cn (Baofeng Yang), zhaoxin@hrbmu.edu.cn (Xin Zhao).
Peer review under the responsibility of Chinese Pharmaceutical Association and Institute of Materia Medica, Chinese Academy of Medical Sciences.

https://doi.org/10.1016/j.apsb.2025.11.014

Liver-brown fat communication;
Lipotoxicity;
Hepatic steatosis

obese mice. These findings establish BHB as a critical link between BAT MLC and the systemic metabolic benefits, highlighting the RAB10−PLIN5 complex as a therapeutic target for obesity and hepatic steatosis. Furthermore, this work underscores the broader significance of cold-induced metabolic adaptations for combating metabolic diseases.

1. Introduction

Obesity is a growing global health crisis, closely linked to type 2 diabetes (T2D), metabolic dysfunction-associated steatotic liver disease (MASLD), and other cardiometabolic disorders[1-3]. Central to these metabolic disturbances is adipose tissue, which plays a dual role: white adipose tissue (WAT) serves as an energy reservoir. In contrast, brown adipose tissue (BAT) can burn stored fat through its thermogenic capacity, while also consuming glucose[4-7]. BAT's ability to dissipate energy *via* thermogenesis, particularly under cold exposure, has garnered attention as a promising strategy to combat obesity and related metabolic diseases[8]. In rodents, cold-induced activation of BAT and mediated by heightened sympathetic nervous system activity and β-adrenergic receptor signaling, improves systemic energy expenditure, insulin sensitivity, and glucose homeostasis[9]. However, the precise metabolic mechanisms underlying these benefits remain poorly understood.

Emerging evidence indicates that cold exposure induces dynamic metabolic adaptations, including alterations in circulating metabolites with protective effects[10-12]. Among these adaptations, the mitochondrial−lipid droplet contact (MLC) in BAT, which is a crucial interface for lipid trafficking and fatty acid β-oxidation, plays a pivotal role[13-17]. However, the molecular mediators governing MLC dynamics in BAT have yet to be fully elucidated.

Perilipin 5 (PLIN5), a lipid droplet-associated protein, facilitates FA transfer to mitochondria under metabolic stress and has been implicated in MLC formation in multiple tissues[8,18,19]. Similarly, Rab proteins, a family of small GTPases involved in organelle trafficking and interaction, have emerged as regulators of MLC[20-23]. For instance, RAB8A has been shown to coordinate MLC formation in skeletal muscle by interacting with PLIN5[24]. However, the role of RAB proteins in BAT MLC dynamics and their integration into thermogenic pathways remain unclear.

In this study, we identify RAB10 as a novel regulator of MLC in BAT, uncovering a critical role for β-hydroxybutyrate (BHB), a cold-induced metabolite, in modulating the interaction of RAB10 with PLIN5. Specifically, BHB directly targets at the GLY-67 residue of RAB10, enhancing its interaction with PLIN5 to form the RAB10−PLIN5 complex, thereby promoting MLC formation and optimizing BAT function. These findings provide mechanistic insights into BAT metabolism and identify the RAB10−PLIN5 axis as a potential therapeutic target for combating obesity, T2D, and MASLD.

2. Materials and methods

2.1. Cell culture and reagents

3T3-L1 cells were obtained from Shanghai Zhong Qiao Xin Zhou Biotechnology and cultured in Dulbecco's modified Eagle's medium (DMEM) supplemented with 10% fetal bovine serum (FBS, Biological Industries, Israel) and 1% penicillin−streptomycin.

Mouse primary hepatocytes (MPHs) were isolated from the livers of 8-week-old male C57BL/6J mice using standard procedures. Mice were anaesthetized and perfused *via* portal vein with freshly prepared buffer, followed by digest buffer (collagenase IV, Worthington, NJ, USA). Subsequently, the perfused livers were excised. Viability was determined by trypan blue exclusion assay (Corning, Rochester, NY, USA). MPHs were cultured in DMEM supplemented with 10% fetal bovine serum, 10 mmol/L insulin (HY-P0035, MCE, USA), and 10 mmol/L dexamethasone (HY-14648, MCE, USA).

Subcutaneous white and brown adipose tissues (WAT and BAT) were isolated from 3−4-week-old male C57BL/6J mice. The tissues were minced and digested in 2 mL of 10 mmol/L HEPES solution (Gibco, 15630-080) containing 2 mg/mL type II collagenase (Sigma, C6885) at 37 °C for 30 min. After digestion, the tissues were filtered through a 100 μm filter and centrifuged. Stromal-vascular (SV) cells were collected and cultured in DMEM with 10% FBS.

For differentiation of 3T3-L1 and SV cells into mature brown adipocytes, cells were cultured to confluence (Day 1), after which the medium was replaced with differentiation medium containing 20 nmol/L insulin (MCE, #HY-P0035), 1 μmol/L rosiglitazone (Sigma, #R2409), 0.5 mmol/L isobutylmethylxanthine (Sigma, #17078), 125 μmol/L indomethacin (Sigma, #17378), 5 μmol/L dexamethasone (Sigma−Aldrich), and 1 nmol/L triiodothyronine (T3, MCE, #HY-A0070AG). After 3 days, the medium was replaced with differentiation medium containing 20 nmol/L insulin and 1 nmol/L T3, and after 2 additional days, the cells were maintained in normal medium and collected for subsequent experiments.

For co-culture experiments, primary hepatocytes were seeded in the upper layer of Transwell inserts, and the induced mature brown adipocytes were plated in the lower layer. For fluorescence staining, the medium from the hepatocytes was removed, mixed 1:1 with fresh medium, and added to the brown adipocyte culture. The co-culture was incubated for 24 h at 37 °C in 5% CO_2.

2.2. Animal maintenance and experiments

All animal care and experimental protocols were approved by the Institutional Review Board (IRB) of the College of Pharmacy, Harbin Medical University (project license number: IRB3073724) and were conducted in compliance with the Chinese Regulations on the Management of Laboratory Animals. All animal studies adhered to the ARRIVE guidelines.

Specific pathogen-free (SPF) male C57BL/6J mice (20−23 g, 8 weeks old) were obtained from Changsheng Biotechnology (Liaoning, China) and housed in a pathogen-free environment with a controlled temperature of 22 ± 2 °C and a 12-h light/dark

cycle. Mice had ad libitum access to food and water throughout the study. For cold exposure experiments, mice were placed in a cold box at 4 °C. Cold exposure was also simulated through subcutaneous injection of the β3-adrenergic receptor agonist CL316243 (1 mg/kg) in the experimental group, while saline was administered to the control group. All animals were fasted for 6 h prior to euthanasia and subsequent experiments.

MASLD mice model: C57BL/6J mice and *ApoE*$^{-/-}$ mice were fed the high-fat, high-cholesterol, and high-fructose (HFHFHC) diet for 12 weeks to induce metabolic dysfunction-associated steatotic liver disease (MASLD). The HFHFHC diet (40 kcal% fat, 20 kcal% fructose, and 2% cholesterol) was obtained from Readydietech Co., Ltd. (Shenzhen, China). C57BL/6J mice were also fed a high-fat, methionine choline-deficient, L-amino acid (HFCDAA) diet (60 kcal% fat, 0.1% methionine, and no added choline) for 8 weeks.

For diet-induced obesity (DIO), C57BL/6J mice were fed a high-fat diet (HFD) for 12 weeks. Control mice were fed a normal diet (ND). Based on the estimated blood volume in mice ($\sim$77.8 mL/kg) and the molecular weight of β-hydroxybutyrate (BHB) (104.1 g/mol), a dosing regimen of 100 mg/kg was calculated to achieve plasma concentrations within the physiological range, considering an oral bioavailability of approximately 60%−70%. Mice on the HFD were divided into three groups: HFD, HFD + BHB (100 mg/kg/week), and HFD + BHB (100 mg/kg/day). Weekly gavage began after 4 weeks on the HFD, and daily gavage started after 9 weeks.

C57BL/6J mice were randomly assigned to the following groups: a control group maintained on a normal chow diet and injected with *AAV8*-sh*NC*, and two experimental groups fed a high-fat diet (HFD) and receiving tail vein injections of either *AAV8*-sh*NC* or *AAV8*-sh*HADHA* (Genechem, Shanghai, China) to achieve liver-specific knockdown of *HADHA*.

2.3. MASLD human patient study

All procedures involving human participants were approved by the Institutional Review Board (IRB) of the College of Pharmacy, Harbin Medical University (Project License Number: IRB3073724, China). MASLD patients and healthy controls were recruited from the Second Affiliated Hospital of Harbin Medical University. Written informed consent was obtained from all participants prior to enrollment.

Inclusion criteria for MASLD patients were as follows.

(1) Absence of excessive alcohol consumption, defined as weekly ethanol intake $\geq$210 g for men and $\geq$140 g for women.
(2) Exclusion of other known causes of hepatic steatosis, including viral hepatitis.
(3) Ultrasonographic evidence of hepatic steatosis accompanied by at least one metabolic risk factor for cardiovascular disease (*e.g.*, fasting blood glucose $\geq$6.1 mmol/L or fasting triglycerides $\geq$1.7 mmol/L).

All study procedures conformed to the ethical principles outlined in the Declaration of Helsinki.

2.4. Histopathologic analysis

Paraffin-embedded tissue sections from the liver, white adipose tissue (WAT), brown adipose tissue (BAT), and heart were subjected to hematoxylin and eosin (H&E) staining for general histological assessment. Liver sections were additionally stained with Oil Red O to evaluate lipid accumulation. For immunohistochemical analysis, liver sections were stained with an anti-HADHA antibody to detect hepatic HADHA protein expression.

2.5. Doppler ultrasound

Doppler ultrasound (VINNO Technology, Suzhou, China) was used to measure the internal diameter of the aortic outflow tract, the forward-to-backward aortic flow ratio, and the aortic diameter to assess vascular conditions. The oblique diameter of the right lobe of the liver was measured to evaluate liver lesions, and the contractile capacity of the heart was assessed through parameters such as ejection fraction (EF, %) and fractional shortening (FS, %).

2.6. Fatty acid oxidation (FAO) assay

Hepatic FAO capacity was measured using a Fatty Acid Oxidation Colorimetric Assay Kit (E-BC-K784-M, Elabscience, USA), according to the manufacturer's instructions. Briefly, liver tissues were homogenized, and the supernatant was collected following centrifugation. A portion of the supernatant was used to determine protein concentration, while the remaining aliquot was subjected to FAO analysis. Optical density (OD) was measured at 450 nm using a microplate reader. FAO activity was calculated based on the standard curve, taking into account the dilution factor and protein concentration.

2.7. WGA staining

Heart tissue was fixed with 4% formaldehyde, then dehydrated, transparented, and embedded in paraffin. Cut into 6 μmol/L thick samples, they were deparaffinised, antigenically repaired, and stained with 50 μg/mL WGA-FITC (GTX01502, GeneTex, TX, USA).

2.8. RNA sequencing combined with metabolic sequencing

Brown adipose tissue and plasma from mice were subjected to mRNA sequencing and metabolomics analyses, respectively, and the results were subjected to combined transcriptomic and metabolomic analyses. The RNA sequencing libraries were then prepared and sequenced by Shanghai Origin-Gene Biomedical Technology Co., Ltd. Metabolome screening criteria: P value < 0.05, VIP>1, $\log_2$FC > 0 or $\log_2$FC < 0. Transcriptome screening criteria: P value < 0.05, $\log_2$FC > 1 or $\log_2$FC < -1. Combined analysis screening criteria: Combined-P value < 0.05.

2.9. Acetyl-CoA and BHB content assays

Acetyl-CoA levels were quantified using a commercial Acetyl-CoA content kit (#JL-T1295, Jianglai, China) according to the manufacturer's instructions. BHB content in serum and cell lysates was measured using a mouse BHB content assay kit (#BC5085, Solarbio, China) and a β-hydroxybutyrate Colorimetric Assay Kit (#E-BC-K785-M, Elabscience, China).

2.10. RNA isolation and real-time quantitative RT-PCR

Total RNA was isolated from cultured 3T3-L1 cells and SV induction into mature brown adipocyte cells using TRIzol, and the

Concentration of the extracted RNA was measured with a NanoDrop 8000 (ThermoFisher Scientific, USA). Quantitative real-time PCR assays were performed on an Applied Biosystems 7500 Fast Real-Time PCR System (Applied Biosystems, USA). Primer sequences are shown in Supporting Information Table S1.

2.11. Western blotting

Proteins were lysed using RIPA buffer. Proteins were quantified using the BCA Protein Assay Kit. Incubate the primary antibody overnight at 4 °C and then incubate with the fluorescently labelled secondary antibody for 1 h at room temperature away from light. Images were acquired using the Odyssey CLx Infrared Imaging System.

2.12. BAT transplantation

Mice were anesthetized, and the skin in the scapular region was prepared by hair removal and disinfection. An 'H'-shaped incision was made on the back, extending horizontally at both ends. The skin was then opened to expose the adipose tissue between the scapulae. Brown adipose tissue (BAT) was isolated by removing the surrounding white adipose tissue, and blunt dissection was used to excise the BAT from the underlying muscle. Sham-operated mice underwent the same procedure; however, instead of excising BAT, their peripubic fat pads were exposed and closed.

2.13. Oil red O staining

3T3-L1 and SV cells, differentiated into mature brown adipocytes, were treated with varying doses of BHB, according to experimental groups. Cells were stained with Oil Red O (#G1261, Solarbio, China) for 15 min. Images were captured using a Leica Microsystems microscope (Leica, Solms, Germany) or observed under a fluorescence microscope (BX53, Olympus, Japan).

2.14. Construction and transfection of siRNA

siRNAs targeting HADHA, PLIN5, and RAB10, as well as overexpression plasmids including mCherry-RAB10, His-PLIN5, Flag-RAB10, and mutant forms of *RAB10*, were synthesized by HonorGene (Changsha, China). Brown adipocytes were seeded in six-well plates and transfected with 250 μL of a siRNA−Lipofectamine 2000 mixture per well. For primary hepatocytes, transfection was carried out using Lipofectamine RNAiMAX reagent (Life Technologies), according to the manufacturer's protocol. Cells were incubated with the transfection complexes for 6 h, followed by replacement with complete medium containing serum and further incubation for 48 h before subsequent analyses.

2.15. Immunofluorescence

Mitochondria and lipid droplets were labeled with MitoTracker Red (#167095-09-2, Invitrogen, USA) and Bodipy 493/503 (#GC42959, GLpBio, USA), respectively. For fluorescent FAs tracking, mature brown adipocytes were incubated with 1 mmol/L Bodipy 558/568 C12 (#MX5402, Maokang Biotechnology, China) in DMEM containing 10% FBS for 12 h. After washing with PBS to remove excess C12, the cells were labeled with MitoTracker Green (#201860-17-5, Invitrogen, USA) for mitochondrial staining or with Bodipy 493/503 for lipid droplet labeling. To examine co-localization, mCherry-RAB10 plasmid transfection was performed alongside TOM20 for mitochondrial labeling, or mCherry-RAB10 and His-PLIN5 plasmid co-transfection was used for RAB10-PLIN5 co-localization analysis. All images were analyzed using a fluorescence microscope (Olympus, Tokyo, Japan).

2.16. Mitochondrial respiratory measurement

Mitochondrial respiratory function of brown adipocytes was measured using high-resolution respirometry (Oxygraph-2k, Oroboros Instruments, Innsbruck, Austria). The protocol involved recording routine respiratory rates, followed by induction of a non-phosphorylating leak state with oligomycin (0.5 μmol/L, #495455, Sigma−Aldrich). After stabilisation, FCCP (1 μmol/L, #C2920, Sigma−Aldrich) was added to assess maximum respiratory capacity. Finally, rotenone and antimycin A were added to measure non-mitochondrial respiration, reflecting residual oxygen consumption independent of mitochondrial activity.

2.17. Flow cytometry analysis

To assess mitochondrial activity, brown adipocytes were stained with MitoSox (5 μmol/L) for 15 min in the dark, and the percentage of MitoSox-positive cells was quantified using a Beckman CytoFLEX flow cytometer (Beckman, CA, USA).

2.18. Cell mitochondrial DNA extraction

Mitochondrial DNA was isolated using the Cells Mitochondrial DNA Extraction Kit (#XH008, Biomart, China) according to the manufacturer's instructions. Briefly, cells were digested with trypsin to collect mitochondrial precipitates, and treated with DNase to remove nuclear DNA. The resulting mitochondrial DNA was then extracted and dissolved using TE buffer. The isolated mitochondrial DNA was used for subsequent copy number assays.

2.19. Mitochondrial DNA copy number assay

Mitochondrial DNA copy number was quantified using the Mitochondrial DNA Copy Detection Kit (Shanghai Yihe Application Biological Technology Co., Ltd.). Two-color fluorescence qPCR (FAM + HEX) was used, with a standard curve generated from known mitochondrial DNA standards provided in the kit. The mitochondrial DNA copy number of brown adipocytes was determined by absolute quantification using the corrected calibrators.

2.20. OGTT and ITT

After 10 weeks on a high-fat diet (HFD), oral glucose tolerance tests (OGTT) were performed following an 8 h fast. Blood glucose levels were measured at baseline, 15, 30, 60, and 120 min after oral administration of a 0.5 g/mL D-glucose solution (Sigma−Aldrich). The insulin tolerance test (ITT) was conducted one week after the OGTT.

2.21. Measurement of TC, TG, and NEFA levels

Plasma levels of total cholesterol (TC), triglycerides (TG), and non-esterified fatty acids (NEFA), as well as hepatic TC and TG contents, were quantified using commercially available assay kits, following the manufacturers' instructions.

2.22. Electron microscopy

Brown adipose tissue was rapidly excised from each group of mice. The tissue was cut into 3 mm × 3 mm sections and fixed in 2% glutaraldehyde (#AWI0097, abiowell, China) for 6 h. The fixative was discarded and washed with PBS buffer for 6 h. Samples were fixed in 1% osmium tetroxide (#AWI0136, Abiowell, China) for 1 h, then dehydrated in ethanol and embedded in epoxy resin (#M25514, Meryer, China). Thin sections were prepared using a Leica ultrathin sectioning machine (Leica UC-7), stained with lead citrate and observed using a Nippon Electron JEM1400 transmission electron microscope.

2.23. Specific pupylation as IDEntity reporter (SPIDER) assay

3T3-L1 cells were differentiated into mature brown adipocytes, and protein extraction was performed using NP40 lysis buffer containing protease and phosphatase inhibitors. The SPIDER assay was performed as described previously[61]. Biotin-cadaverine labeling of BHB was used for detection. For the experimental group, 0.1 μmol/L biotin-cadaverine-labeled BHB was added to 3 mg of protein in cell lysates, and the volume was adjusted to 6 mL with reaction buffer. The mixture was incubated overnight at 4 °C. Following incubation, SA-Pup4 was added at a final concentration of 0.1 μmol/L and incubated for 20 min at room temperature. ATP (5 mmol/L) and PafA (0.1 μmol/L) were added and incubated for 30 min at 37 °C. After incubation, 4.8 g urea was added, and the reaction was processed by adding 0.1% Tween-20 and 100 μL biotin-agarose for 2 h at room temperature. The reaction was centrifuged, washed, and centrifuged again to remove the supernatant.

Mass spectrometry identified 1051 protein molecules, and 77 interacting proteins met the thresholds (unique peptides ≥2, fold change ≥1.5) across two replicates.

2.24. Pull down assay

Biotinylated protein pull-down assays were performed using a Biotinylated Protein Pull-Down Kit (#P0658S, Beyotime, China). Streptavidin magnetic beads were mixed with binding buffer, and 50 μg biotin-labeled BHB was added to the beads, incubated for 30 min on an orbital shaker. After incubation, the beads were washed, blocked with biotin blocking solution for 10 min, and incubated with sample lysate (400 μL) for 2 h at 4 °C. After the incubation, streptavidin magnetic beads were resuspended in elution buffer, and the target protein was eluted by shaking for 10 min.

2.25. Surface plasmon resonance (SPR) assay

Protein conjugation was performed using 1-ethyl-3-(3-dimethylaminopropyl) carbodiimide (EDC, Cytiva) and *N*-hydroxysuccinimide (NHS, Cytiva) to immobilize the protein on a chip. The ligand protein was diluted to 50 μg/mL in sodium acetate and immobilized at a flow rate of 10 μL/min. The channel was blocked with ethanolamine at 10 μL/min. Protein−analyte interaction tests were conducted, and binding and dissociation constants were calculated using the Biacore Insight evaluation software (Cytiva, Marlborough, MA, USA).

2.26. CETSA assay

The cellular thermal shift assay (CETSA) was employed to detect the intracellular binding status of target proteins by assessing changes in protein thermal stability. Cells were digested with trypsin, incubated in PBS with phosphatase inhibitors, and subjected to multiple freeze−thaw cycles. Following centrifugation, the supernatant was divided and incubated with DMSO or BHB at room temperature for 3 h. The samples were heated at increasing temperatures (37 to 61 °C) for 4 min, centrifuged, and the supernatant was analyzed by Western blot after boiling.

2.27. DRATS assay

The DARTS assay was used to confirm the binding of BHB to RAB10. Cells were lysed, and protein concentrations were determined using a BCA assay. The lysates were incubated with varying concentrations of BHB or DMSO for 3 h, followed by pronase treatment for 15 min. After protein denaturation by heating, the samples were analyzed by Western blot.

2.28. Molecular docking

The protein structure was downloaded from AlphaFold (https://alphafold.ebi.ac.uk/entry/P61027), and 3D structures were prepared using PyMOL. The chemical structure of the ligand was obtained from PubChem (https://pubchem.ncbi.nlm.nih.gov/). Docking was performed using the CB-DOCK2 online server (https://cadd.labshare.cn/cb-dock2/php/blinddock.php), which utilizes artificial neural networks for cavity detection and AutoDock Vina for docking. The stability of the ligand-receptor binding was assessed through force analysis using PLIP (https://plip-tool.biotec.tu-dresden.de/plip-web) and visualized in PyMOL.

2.29. Molecular dynamics simulations

Molecular dynamics simulations were conducted using Amber24 with the FF14SB force field and the TIP3P water model. The system was energy minimized, followed by NVT and NPT equilibration (200 and 100 ps, respectively). The system temperature was maintained at 300 K, and pressure was controlled at 1 bar. Simulations were run for 50 ns, and parameters such as RMSD, RMSF, radius of gyration, hydrogen bonds, and binding free energy were analyzed using Cpptraj and Python.

2.30. Co-immunoprecipitation assays

Co-immunoprecipitation (Co-IP) was performed using His-PLIN5 or FLAG-RAB10 overexpression plasmids in brown adipocytes, followed by 48 h of incubation. Cells were lysed using IP lysis buffer, and 25 μg of His or Flag antibody was added per reaction. The mixture was incubated with antibody-coated beads overnight at 4 °C. The bound complexes were eluted using elution buffer and analyzed by Western blot. Information on reagents and antibodies used in this article can be found in Supporting Information Table S2.

2.31. Statistical analysis

Data were expressed as mean ± standard error of mean (SEM). Statistical analyses were performed using GraphPad Prism version

8.0. Differences between two groups were assessed using Student's *t*-test, while one-way or two-way ANOVA was applied for multiple group comparisons, followed by Dunnett's or Tukey's *post hoc* tests. Repeated measures ANOVA was used for datasets normalized to a control value of 1, without SEM. *P*-values less than 0.05 were considered statistically significant.

3. Results

3.1. Effects of acute and chronic cold exposure on various organs

To systematically investigate the impact of cold exposure on various tissues and organs, we exposed C57BL/6J mice to acute cold (4 °C for 6, 12, or 24 h) and chronic cold (4 °C for 3, 7, 14, 20, or 30 days), with control mice maintained at 23 °C (Fig. 1A). Acute cold exposure increased the weight of BAT significantly after 24 h, with progressive BAT weight gain observed during chronic exposure (Fig. 1B and C). Conversely, epididymal white adipose tissue (eWAT) and inguinal white adipose tissue (iWAT) exhibited reduced weight and area within 6 h of cold exposure, with sustained decreases during longer exposure periods (Fig. 1D−G, 1I−K). Interestingly, body weight and tissue weights decreased markedly after 20 days of cold exposure, accompanied by darkened BAT coloration. However, after 30 days, tissue weights increased, and BAT displayed lighter coloration, suggesting adaptive responses (Fig. 1B−G). Hematoxylin and eosin (HE) staining revealed that cold exposure transformed BAT into a multilocular lipid droplet structure, most pronounced at 3 and 20 days, with reduced multilocularity by Day 30 (Fig. 1H). Both eWAT and iWAT showed reduced adipocyte size and number throughout the cold exposure period (Fig. 1I−K, O). Notably, no structural abnormalities were observed in liver tissue during the 30-day exposure (Fig. 1L). The ratio of liver weight-to-body weight (LW/BW) showed no significant change during cold exposure (Supporting Information Fig. S1A). The heart weight-to-body weight (HW/BW) ratio increased during acute exposure, chronic cold reduced this ratio (Fig. S1B). At 30 days, hypertrophy of cardiac cells was evident, confirmed by HE staining and wheat germ agglutinin staining (Fig. 1M and N). Plasma markers of cardiac (LDH) and liver (ALT, AST) injury remained within normal ranges throughout the exposure (Fig. S1C−S1E). Doppler ultrasound analysis showed no significant changes in the diastolic and systolic diameters of the aortic outflow tract or blood flow ratios during acute cold exposure. However, at 30 days, both the aortic diameter difference and forward-to-reverse blood flow ratio decreased significantly (Fig. S1F−S1K). Importantly, ejection fraction (EF, %) and fractional shortening (FS, %) of the heart declined modestly during cold exposure but remained within normal physiological limits until 20 days (Fig. 1P and Q). Cold exposure induces significant alterations in adipose tissue, including increased BAT mass, reduced white adipocyte size and number, and BAT multilocularity, peaking at 20 days. These effects are accompanied by transient reductions in body and organ weights without pathological changes in liver or heart structure. After 30 days, adaptive mechanisms appear to mitigate these changes, normalizing organ weights and BAT morphology. These findings suggest that cold exposure enhances BAT activity and reduces white adiposity without inducing deleterious effects on key metabolic organs. To understand the molecular adaptations of BAT during cold exposure, transcriptomic profiling was performed on BAT from control mice (23 °C) and cold-exposed mice (4 °C for 3 days). A total of 779 differentially expressed genes (DEGs) were identified, with 419 genes upregulated and 360 downregulated in cold-exposed mice (Fig. 1R, Supporting Information Fig. S2A). GO functional enrichment analysis of upregulated genes highlighted pathways associated with lipid droplets, fatty acid metabolism, and lipid metabolic processes, alongside basic cellular processes such as nucleotide binding and cytokine regulation (Fig. S2B). A heatmap of gene expression revealed significant upregulation of genes involved in fatty acid oxidation (FAO), including *Hadha*, *Ucp1*, and *Pdk1*, mitochondrial dynamics (*Acaa1b*, *Slc25a20*), while genes related to fatty acid synthesis and lipid droplet were downregulated (Fig. S2C). GSEA analysis shows cold exposure significantly affects fat metabolism-related pathways (Fig. S2D−S2F). These findings underscore the metabolic reprogramming of BAT under cold exposure.

3.2. BHB production involves communication between the liver and BAT during cold exposure

Plasma metabolomic analysis was performed to complement the transcriptomic data. Cold exposure results in significant changes in metabolites (Fig. S2G). Functional pathway enrichment and heatmap analyses identified β-hydroxybutyrate (BHB) as one of the most significantly altered metabolites and lipid metabolism as the primary pathway affected (Fig. 2A−C, Fig. S2H). As a ketone body predominantly generated by hepatic FAO, BHB serves as an alternative energy source, transported *via* the bloodstream to tissues such as the brain, muscle, and heart for energy metabolism. A combined analysis of DEGs and plasma metabolites identified 39 genes implicated in regulating metabolite changes, with hydroxyacyl-CoA dehydrogenase trifunctional multienzyme complex subunit alpha (*Hadha*) emerging as a critical regulator of BHB (Fig. 2D, Fig. S2I). HADHA, a component of the mitochondrial trifunctional enzyme complex, plays a pivotal role in the β-oxidation of long-chain fatty acids, primarily in BAT and the liver—key tissues for fatty acid metabolism and thermogenesis[25-28]. Plasma BHB levels were significantly elevated in both acutely and chronically cold-exposed mice compared to controls (Fig. 2E). To simulate cold-induced BAT activation, mice were treated with the β3-adrenergic receptor agonist CL-316,243 (1.0 mg/kg) or saline for 3 or 7 days[29]. Plasma BHB levels were significantly increased in agonist-treated mice, mirroring the effects observed under cold exposure (Fig. 2F). Consistent with metabolomic findings, cold exposure significantly upregulated mRNA levels of *Hadha* in BAT, further supporting its role in BHB production and fatty acid metabolism (Fig. 2G). Western blot analysis of BAT from mice exposed to cold for 3 and 20 days showed a significant increase in UCP1 and HADHA protein expression compared to controls (Fig. 2H and I). This aligns with transcriptomic findings, reinforcing the role of HADHA in the oxidation of long-chain fatty acids to produce acetyl-CoA, a precursor for BHB synthesis[30,31]. These results suggest that cold-induced increases in circulating BHB levels may depend on enhanced HADHA expression in BAT. To investigate the contribution of BAT to BHB production, BAT-transplanted and sham-operated C57BL/6J mice were exposed to cold for 3 days. ELISA revealed that circulating BHB levels remained elevated even after BAT removal, indicating that other tissues contribute to BHB production during cold exposure (Fig. 2J). Given that the liver is a primary site for BHB synthesis[32], we examined hepatic

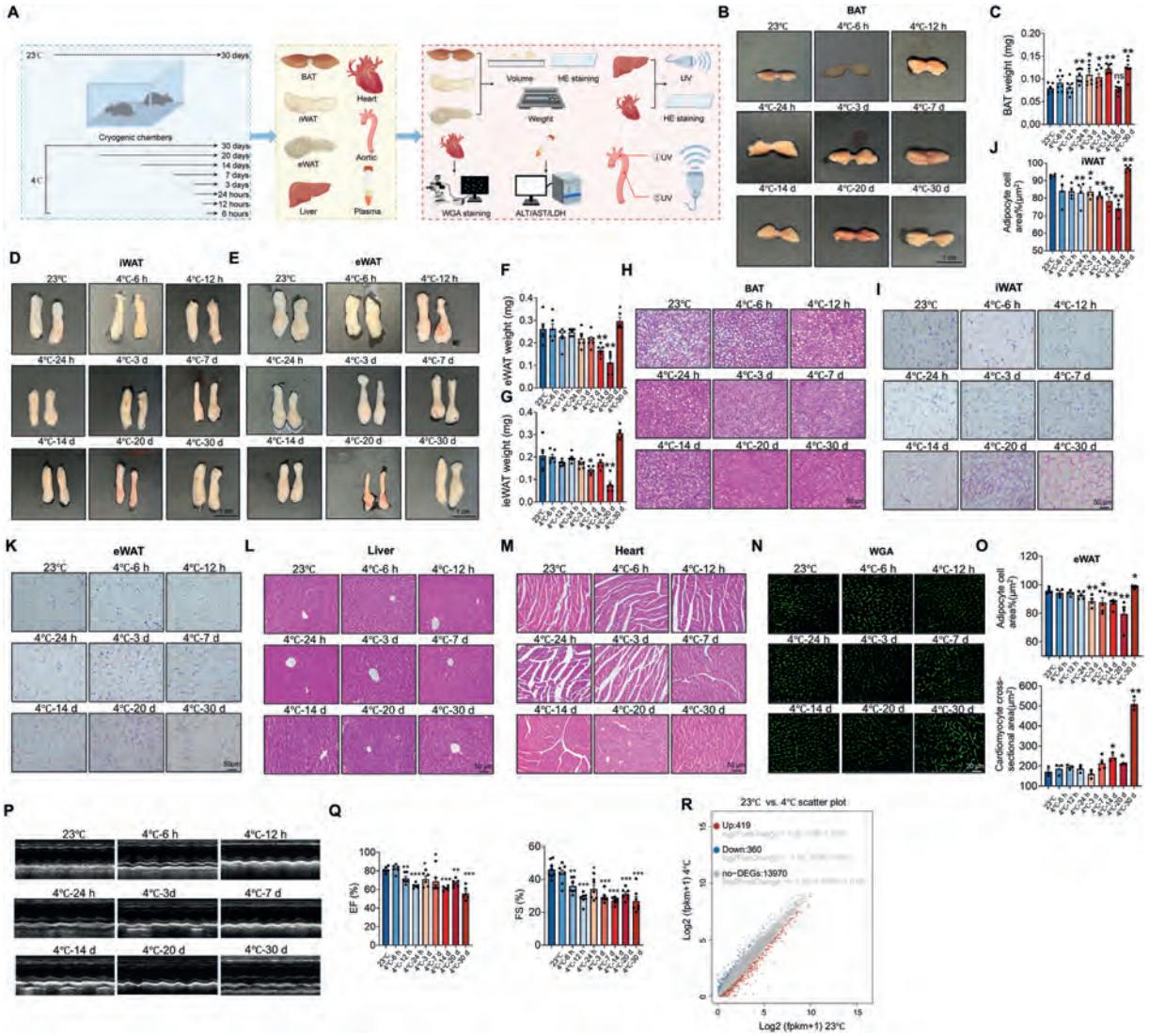

Figure 1 Effects of acute and chronic cold exposure on various organs. (A) Experimental grouping and process. (B−E) Representative plots of BAT, iWAT, and eWAT in each group of mice. $n = 6$ in each group. Scale bar: 1 cm. (C, F, G) Weight statistics of BAT, eWAT, and iWAT in each group of mice. $n = 6$ in each group. (H−M) Representative images of H&E staining of BAT, iWAT, eWAT, liver, and heart sections from mice. $n = 6$ in each group. Scale bar: 50 μm. (N, O) Representative image of WGA staining of mouse heart tissue and their statistics. Scale bar 20 μm. (P, Q) Representative echocardiographic images of each group; changes in ejection fraction (EF, %) and fractional shortening (FS, %) in each group. $n = 6$ in each group. (R) Scatter plot of transcript expression by mRNA sequencing of brown adipose tissue from RT mice and cold-exposed mice. $n = 4$ in each group. Statistical analysis was performed with the randomized block ANOVA. $^{*}P < 0.05$ *vs.* RT, $^{**}P < 0.01$ *vs.* RT, $^{***}P < 0.001$ *vs.* RT. Data are presented as mean ± SEM. BAT, brown adipose tissue; iWAT, subcutaneous white fat; eWAT, epididymal white fat.

HADHA expression during cold exposure. Western blot analysis showed increased HADHA protein levels in the liver of cold-exposed mice (Fig. 2K). And there is increased synthesis of acetyl coenzyme A (Acetyl-CoA) in the liver, which is an important substrate for the synthesis of BHB (Supporting Information Fig. S3A). Overexpression of HADHA in primary hepatocytes elevated BHB levels in the supernatant, while *HADHA* knockdown reduced BHB levels (Fig. 2L, Fig. S3B and S3C). These results confirm that hepatic HADHA plays a critical role in BHB production. Cold exposure leads to an increase in HADHA synthesis in the liver, which in turn leads to an increase in Acetyl-CoA, a substrate for BHB synthesis, and ultimately to an increase in BHB synthesis. To explore the interaction between hepatic BHB production and its utilization in BAT, co-culture experiments were conducted. Primary hepatocytes over-expressing HADHA were co-cultured with mature brown adipocytes. HADHA-overexpressing hepatocytes significantly increased BHB content in brown adipocytes (Fig. 2M and N). This suggests that BHB synthesized in the liver is transported to BAT, where it is utilized for metabolic processes. Our *in vivo* measurements showed that basal plasma BHB levels in mice range from 0.4 to 0.5 mmol/L. Upon cold exposure, circulating BHB levels increased significantly to 0.8−1.2 mmol/L (Fig. 2E). To approximate this physiological range while considering potential local concentration gradients within tissues, we selected 1 mmol/L as the primary concentration for our *in vitro* studies. To further

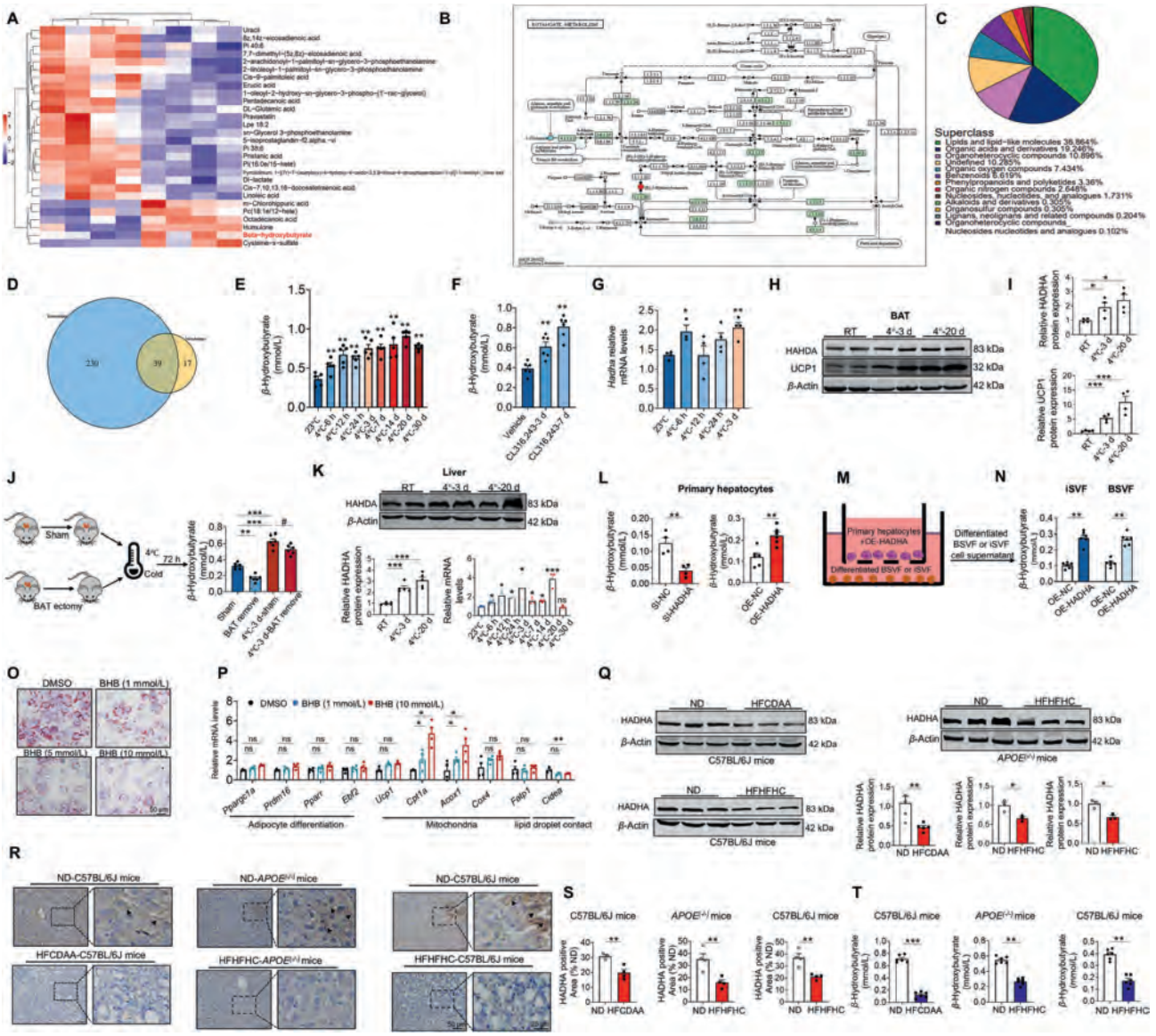

Figure 2 BHB production involves communication between liver and BAT during cold exposure. (A) Significant differential metabolite hierarchical clustering heat map of plasma metabolomics. (B) KEGG map of mouse plasma metabolome function. (C) Hierarchical Clustering Analysis in plasma metabolomics. (D) Wayne plots of differential gene and differential metabolite involvement in pathways analyzed jointly by transcriptome and metabolomics. (E, F) Detection of BHB in plasma of various groups of mice. $n = 6$ in each group. (G) Changes in mRNA levels of HADHA in brown adipose tissue of mice in various groups detected by qPCR. $n = 6$ in each group. $^{*}P < 0.05$ *vs.* RT, $^{**}P < 0.01$ *vs.* RT, $^{***}P < 0.001$ *vs.* RT. (H, I) Western blot analysis of changes in HADHA and UCP1 protein levels in the brown fat of mice in each group. $n = 4$ in each group. $^{**}P < 0.01$ *vs.* RT, $^{***}P < 0.001$ *vs.* RT. (J) After the mice were subjected to BAT transplantation or sham operation, changes in plasma levels of BHB were detected in all groups of mice after 72 h of cold exposure. $n = 6$ in each group. $^{**}P < 0.01$ *vs.* sham, $\#P < 0.05$ *vs* sham+4°C-3d. (K) Western blot and qPCR analysis of HADHA protein and mRNA levels in mouse liver at different time points during cold exposure. $n = 3{-}5$ in each group. $^{*}P < 0.05$ *vs.* RT. (L) Detection of changes in BHB levels in primary hepatocyte lysates following transfection of *HADHA* overexpression or knockdown plasmids into primary hepatocytes. $n = 4, 6$ in each group. $^{**}P < 0.01$ *vs.* NC. (M, N) After transfection of *HADHA* overexpression or knockdown plasmid in primary hepatocytes, co-culture with primary brown adipocyte-derived SVF induced mature brown adipose tissue, or primary subcutaneous white adipose tissue-derived SVF induced mature brown adipocytes, and assay for the content of BHB in brown adipocytes. $n = 6$ in each group. $^{**}P < 0.01$ *vs.* NC. (O) Oil red O staining of lipid changes in mature brown adipocytes after BHB treatment. $n = 6$ in each group. Scale bar: 50 μm. (P) Detection of adipose differentiation, mitochondrial and lipid droplet contact related gene changes in brown adipocytes by qPCR. $n = 4$ in each group. $^{**}P < 0.01$ *vs.* DMSO, ns, no significance. (Q) Western blot detection of HADHA protein in the livers of several MASLD mouse models, including C57BL/6J mice induced by HFCDAA diet for 8 weeks and C57BL/6J and $APOE^{-/-}$ mice induced by HFHFHC diet for 12 weeks. $n = 3, 4$ in each group. $^{*}P < 0.05$ *vs.* ND, $^{**}P < 0.01$ *vs.* ND. (R, S) Immunohistochemical staining of HADHA protein changes in the liver of mice with different MASLD models. $n = 4$ in each group. Scale bar: 50 μm, 25 μm. (T) Changes of BHB in plasma of mice. $n = 6$ in each group. Statistical analysis was performed with one-way ANOVA. $^{**}P < 0.01$ *vs.* ND, $^{***}P < 0.001$ *vs.* ND. Data are presented as mean ± SEM. ND, normal diet; HFHFHC, high-fat, high-cholesterol, high-fructose; HFCDAA, high-fat, methionine choline deficiency diet.

explore dose dependency, we included additional conditions with 5 and 10 mmol/L BHB. To assess the metabolic effects of BHB on brown adipocytes, iWAT-SVF and 3T3-L1 cells were induced to differentiate into mature brown adipocytes and then treated with increasing concentrations of BHB (1, 5, and 10 mmol/L). Oil Red O staining showed that BHB at 10 mmol/L significantly reduced lipid content in brown adipocytes (Fig. 2O and Fig. S3D). Further analysis revealed that BHB treatment enhanced the expression of fatty acid β-oxidation-related genes (*Ppara*, *Cpt1a*, *Mcad*) and decreased lipid droplet contact-related genes (*Cidea*). However, BHB had minimal effects on genes related to adipocyte differentiation, lipogenesis (*Fasn*), or lipolysis (*Atgl*) (Fig. 2P). To evaluate the role of HADHA in metabolic-associated steatotic liver disease (MASLD) and steatohepatitis (MASH), hepatic HADHA expression was assessed in MASLD/MASH mouse models. Liver samples from high-fat diet-induced MASLD/MASH models (HFCDAA, HFHFHC diets, and *APOE*$^{-/-}$ mice) showed reduced HADHA protein expression compared to controls (Fig. 2Q−S). Correspondingly, circulating BHB levels were decreased in MASLD/MASH mice (Fig. 2T). These findings suggest a potential link between reduced hepatic HADHA expression, lower BHB levels, and MASLD progression.

3.3. BHB promotes mitochondrial lipid droplet contact in brown adipocytes

Transcriptomic analysis identified pathways enriched in lipid droplet dynamics, lipid metabolism, and fatty acid metabolism (Fig. S2B). A qPCR assay confirmed that BHB enhances mitochondrial FAO and regulates lipid droplet contact (Fig. 2P). Increased contact between mitochondria and lipid droplets allows FAs stored in lipid droplets to be more easily transported into mitochondria for β-oxidation[33,34]. This unique property of brown adipose tissue contributes to thermoregulation and high energy expenditure[7,35]. Enhanced FAO reduces fat storage, potentially mitigating metabolic diseases such as obesity, MASLD, and atherosclerosis[33,36,37]. White adipocytes are characterized by large, unilocular lipid droplets and few mitochondria, while brown adipocytes contain numerous, multilocular lipid droplets and mitochondria with densely packed cristae[38,39]. Despite these structural differences, the specific effect of BHB on lipid droplet−mitochondria contact (MLC) in brown adipocytes remained unexplored. To evaluate the effects of BHB on MLC, 3T3-L1 cells were differentiated into mature brown adipocytes, followed by BHB treatment at varying concentrations. Mitochondria were stained with Mitotracker Red, and lipid droplets (LDs) were labeled with BODIPY. Fluorescence imaging demonstrated that untreated brown adipocytes displayed typical features of mature brown adipocytes, including multilocular lipid droplets and abundant mitochondria. Some lipid droplets were in contact with mitochondria, while others were distributed externally. BHB treatment led to the disappearance of larger lipid droplets and a dose-dependent increase in mitochondrial-lipid droplet contact (Fig. 3A−C). This contact provides a structural basis for the efficient transfer of fatty acids (FAs) from lipid droplets to mitochondria, enabling their oxidation. To further explore the role of BHB-mediated MLC in FAs transfer, fluorescent labeling of FAs (C12) and mitochondria (Mitotracker Green) or lipid droplets (BODIPY) was performed. Fluorescence imaging revealed that BHB significantly promoted FAs translocation from lipid droplets to mitochondria in a dose-dependent manner (Fig. 3D−F). To confirm these findings, stromal vascular (SV) cells derived from iWAT were differentiated into brown adipocytes. Similar to 3T3-L1-derived brown adipocytes, BHB treatment increased mitochondrial-lipid droplet contact and FAs transfer in a dose-dependent manner (Fig. 3G−I).

3.4. HADHA in hepatocytes regulates BHB to promote fatty acids transfer from LDs to mitochondria in BAT

To examine whether BHB-induced promotion of MLC in brown adipocytes depends on HADHA expression in hepatocytes, primary hepatocytes were engineered to overexpress or knockdown *HADHA*. The supernatant from these hepatocytes was co-cultured with mature brown adipocytes induced from 3T3-L1 cells for 48 h. Co-culture with hepatocytes overexpressing HADHA resulted in smaller lipid droplets and increased MLC in brown adipocytes. In contrast, knockdown of *HADHA* in hepatocytes led to larger lipid droplets and reduced MLC, which was restored by BHB (10 mmol/L) treatment (Fig. 4A and B). Additionally, to evaluate the functional consequence of HADHA modulation on FAs transfer, a Red C12 pulse-tracking assay was performed. Differentiated 3T3-L1 and stromal vascular (SV)-derived brown adipocytes were labeled with Red C12 overnight. Brown adipocytes co-cultured with hepatocytes overexpressing HADHA displayed enhanced FAs transfer from lipid droplets to mitochondria during the pulse period compared to controls (Fig. 4C−E). Fluorescence imaging revealed that Red C12 transitioned from close overlap with lipid droplets to substantial overlap with mitochondria, suggesting efficient mitochondrial FAs uptake. Knockdown of *HADHA* in hepatocytes impaired this FAs transfer, but administration of BHB (10 mmol/L) restored mitochondrial FAs utilization (Fig. 4F−H). To evaluate mitochondrial FAO, a mitochondrial respiration assay was conducted. BHB (10 mmol/L) treatment increased maximal mitochondrial respiration in brown adipocytes, reflecting enhanced FAs oxidation capacity (Fig. 4I−L). Although brown adipocytes possess a high oxidative capacity, excessive reactive oxygen species (ROS) production can lead to cellular damage[40]. Flow cytometric analysis using MitoSOX revealed that co-culture with supernatants from HADHA-overexpressing hepatocytes did not increase intracellular ROS levels in brown adipocytes. Conversely, co-culture with supernatants from *HADHA*-knockdown hepatocytes elevated ROS levels, which were mitigated by BHB (10 mmol/L) treatment (Fig. 4M). Furthermore, co-culture with hepatocytes overexpressing HADHA increased the mitochondrial DNA copy number in brown adipocytes, indicating improved mitochondrial biogenesis and integrity (Fig. 4N and O). BHB enhances MLC in brown adipocytes, facilitating the transfer of FAs from lipid droplets to mitochondria for oxidation. This process boosts mitochondrial FAs oxidation without inducing excessive ROS or cellular damage, demonstrating a protective effect on mitochondrial integrity. These effects are dependent on HADHA expression in hepatocytes, highlighting the critical role of hepatocyte-brown adipocyte crosstalk in lipid metabolism and energy homeostasis.

3.5. BHB targets RAB10 to modulate brown fat-mitochondria lipid droplet contacts

To elucidate the molecular mechanism by which BHB facilitates MLC in brown adipocytes, a biotinylated BHB probe was synthesized, and the Specific Pupylation as IDEntity Reporter (SPIDER) assay was employed to identify BHB's target proteins (Fig. 5A and B, Supporting Information Fig. S4A). Among 77

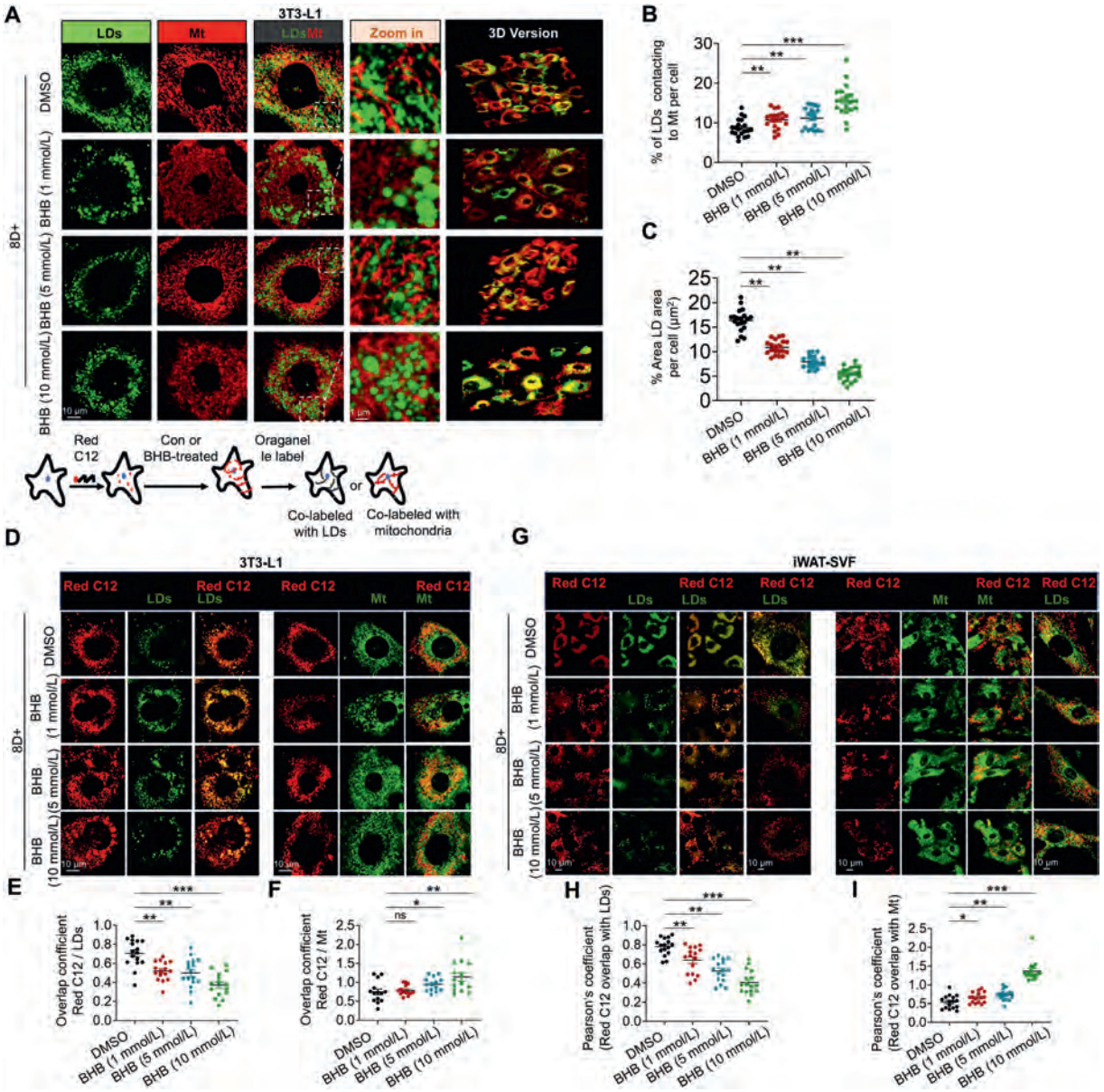

Figure 3 BHB promotes mitochondrial lipid droplet contact in brown adipocytes. (A–C) The percentage of lipid droplets in contact with mitochondria and the area of lipid droplets in brown adipocytes treated with different concentrations of BHB were counted by Mitotracker Red staining of mitochondria and BODIPY staining of lipid droplets. $n = 20$ in each group. (D) FAs was detected by C12, while mitochondria were stained with Mitotracker Green or lipid droplets were stained with BODIPY in mature brown adipocytes induced by 3T3-L1 cells. $n = 14, 15$ in each group. (E, F) Statistics on the localization of FAs to mitochondria or lipid droplets in brown adipocytes after BHB treatment. $n = 14, 15$ in each group. (G–I) In SVF-induced mature brown adipocytes, FAs were detected by C12, and mitochondria were stained with Mitotracker Green or lipid droplets were stained with BODIPY, and statistics of FAs localization in mitochondria or lipid droplets of brown adipocytes after BHB treatment. Scale bar: 10 μm. Statistical analysis was performed with one-way ANOVA. $n = 14, 15$ in each group. $^{*}P < 0.05$ *vs.* DMSO, $^{**}P < 0.01$ *vs.* DMSO, $^{***}P < 0.001$ *vs.* DMSO. Data are presented as mean ± SEM.

enriched proteins (fold change >1.5, identified peptides >2), RAB10 emerged as a top candidate closely associated with organelle interactions, ranking among the top three in binding capacity (Fig. 5C and D). Fluorescence imaging revealed significant co-localization of mCherry-RAB10 with mitochondria in 3T3-L1-induced mature brown adipocytes (Fig. 5E). Pull-down experiments using biotin-labeled BHB confirmed RAB10 as a binding partner (Fig. 5F). To characterize the interaction further, surface plasmon resonance (SPR), cellular thermal shift assay (CETSA), drug affinity responsive target stability (DARTS), and molecular docking analyses were conducted. SPR results showed that BHB binds RAB10 with an equilibrium dissociation constant (K_D) of 3.29×10^{-6} M, indicating a strong affinity (Fig. 5G, Fig. S4B). CETSA experiments showed that BHB (10 mmol/L) treatment improved the protein stability of RAB10 (Fig. 5H and I). Consistently, the DARTS results also showed that BHB significantly contributed to the stability of RAB10 during streptavidin-induced degradation. In addition, the stability of RAB10

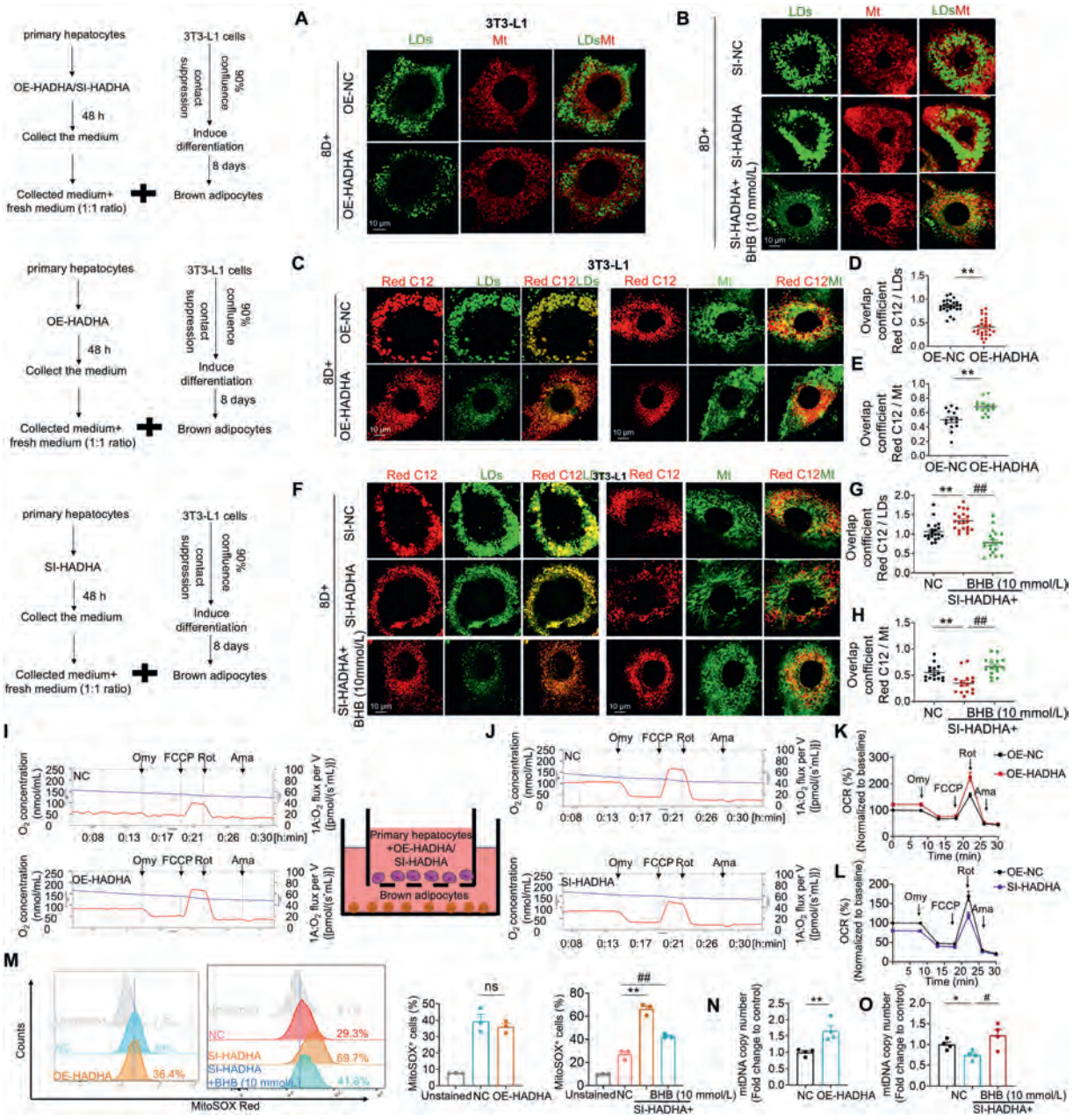

Figure 4 HADHA in hepatocytes regulates BHB to promote fatty acids transfer from LDs to mitochondria in BAT. (A) After HADHA overexpression of primary hepatocytes, their medium was collected and co-cultured with mature brown adipocytes induced from 3T3-L1 cells for 48 h. Mitochondria of mature brown adipocytes were visualised by Mitotracker Red staining as well as lipid droplets by BODIPY staining. $n = 13$ in each group. (B) After HADHA knockdown of primary hepatocytes, their medium was collected and co-cultured with mature brown adipocytes induced from 3T3-L1 cells for 48 h. Mitochondria of mature brown adipocytes were visualized by Mitotracker Red staining as well as lipid droplets by BODIPY staining. $n = 20$ in each group. (C−E) After overexpression of HADHA in primary hepatocytes, their medium was collected and co-cultured with mature brown adipocytes induced from 3T3-L1 cells, and brown adipocyte FAs were detected by C12 and mitochondria were stained with Mitotracker Green or lipid droplets were stained with BODIPY. Statistics of FAs localisation to mitochondria or FAs localisation to LDs. $n = 15, 24$ in each group. (F−H) Brown adipocyte FAs was detected by C12 and mitochondria were stained with Mitotracker Green or lipid droplets were stained with BODIPY. Statistics of FAs localisation to mitochondria or FAs localisation to LDs. $n = 15, 19$ in each group. (I−L) Raw images and statistics of mitochondrial respiration assay in mature brown adipocytes after co-culture with primary hepatocytes. $n = 3$ in each group. (M) MitoSOX staining in mature brown adipocytes after co-culture with primary hepatocytes detected by flow cytometry. $n = 3$ in each group. (N, O) Detection of mitochondrial DNA copy number in mature brown adipocytes after co-culture with primary hepatocytes. $n = 4$ in each group. Scale bar: 10 μm. Statistical analysis was performed with one-way ANOVA. $^{*}P < 0.05$ *vs.* NC, $^{**}P < 0.01$ *vs.* NC, $^{\#}P < 0.05$ *vs.* SI-HADHA, $^{\#\#}P < 0.01$ *vs.* SI-HADHA, ns, not significant. Data are presented as mean ± SEM.

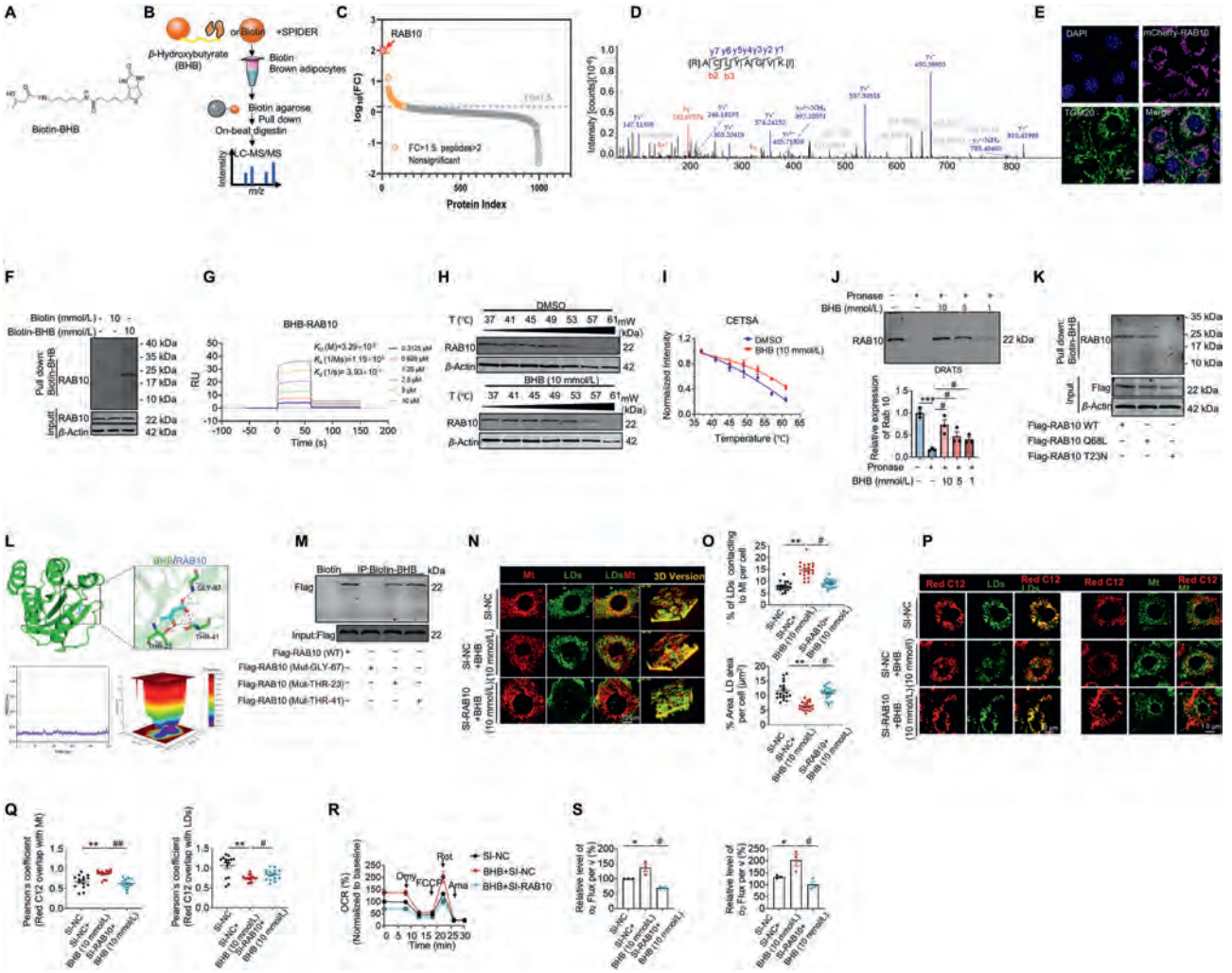

Figure 5 BHB targets RAB10 to modulate brown fat−mitochondria lipid droplet contacts. (A) Chemical structure of biotin-labelled BHB. (B) Flowchart of the SPIDER experiment to obtain reciprocal proteins of BHB in brown adipocytes. (C) Fold change (FC) scatterplot for SPIDER assay using mature brown adipocyte lysate. (D) Mass spectrometry of RAB10 strongly bound to BHB in brown adipocytes in the SPIDER assay. (E) Co-localization of mCherry-RAB10 with TOM20-labelled mitochondria in brown adipocytes detected by immunofluorescence. $n = 6$ in each group. (F) Pull down detection of Biot-BHB binding to RAB10 in brown adipocytes. $n = 3$ in each group. (G) Surface plasmon resonance (SPR) detection of BHB binding to RAB10. (H, I) Cellular thermal shift assay (CETSA) detection of BHB binding to RAB10. $n = 3$ in each group. (J) Binding of BHB to RAB10 as detected by the drug affinity responsive target stability (DARTS) assay. $n = 3$ in each group. $^{***}P < 0.001$ *vs.* Control, $^{\#}P < 0.05$ *vs.* Pronase. (K) The binding of BHB to RAB10 was detected by pull down after transfection of *RAB10* wild-type plasmid, *RAB10* active GTP form of Flag-RAB10-Q68L plasmid, and inactive GDP form of Flag-RAB10-T23N plasmid in brown adipocytes, respectively. $n = 3$ in each group. (L) Molecular docking predicts the binding site of BHB and RAB10, and a schematic of the molecular dynamics simulation of BHB and RAB10. (M) The top three possible binding sites for the molecular docking predictions of *BHB* and *RAB10* were mutated and transfected into brown adipocytes, and the binding sites were later detected by pull-down assay. $n = 3$ in each group. (N, O) After knockdown of *RAB10* in brown adipocytes, changes in mitochondrial and lipid droplet effects of BHB on brown adipocytes were detected by Mitotracker and BODIPY staining. $n = 20$ in each group. (P, Q) C12 and mitochondria were stained with Mitotracker Green, or lipid droplets were stained with BODIPY. Statistics of FAs localization to mitochondria or FAs localization to LDs. $n = 15-16$ in each group. (R, S) Raw images and statistics of mitochondrial respiration assay in mature brown adipocytes. $n = 3$ in each group. Scale bar: 10 μm. Statistical analysis was performed with one-way ANOVA. $^{**}P < 0.01$ *vs.* NC, $^{\#}P < 0.05$ *vs.* SI-NC + BHB, $^{\#\#}P < 0.01$ *vs.* SI-NC + BHB. Data are presented as mean ± SEM.

increased with increasing concentration of BHB (Fig. 5J). RAB10, a small GTPase, regulates intracellular membrane trafficking by transitioning between GDP-bound inactive and GTP-bound active states. Pull-down assays demonstrated that BHB binds selectively to the active GTP-bound form of RAB10 (Fig. 5K). Molecular docking and dynamics simulations revealed that BHB occupies a binding pocket on RAB10, forming hydrogen bonds and hydrophobic interactions with key residues, including GLY-67, THR-23, and THR-41 (Fig. 5L, Fig. S4C). Mutation of GLY-67 abolished BHB's binding to RAB10, highlighting its critical role as the primary binding site (Fig. 5M). Knockdown of *RAB10* in mature brown adipocytes significantly reduced BHB's ability to promote MLC and decreased lipid droplet area (Fig. 5N−Q, Fig. S4D). Furthermore, the enhancement of maximal

mitochondrial respiration by BHB in brown adipocytes was reversed by *RAB10* knockdown (Fig. 5R and S). These findings establish RAB10 as a direct target of BHB, mediating its role in promoting mitochondria−lipid droplet contacts in brown adipocytes. The interaction depends on GLY-67 as the major binding site, highlighting RAB10's essential role in the functional enhancement of mitochondrial activity and lipid droplet dynamics induced by BHB. Furthermore, to assess the physiological relevance of this mechanism, we treated brown adipocytes and primary hepatocytes with free fatty acids (FFA, 250 μmol/L) (Fig. S4F−S4I). FFA exposure increased both the number and size of lipid droplets in brown adipocytes and enhanced lipid accumulation in hepatocytes. Subsequent treatment with BHB (10 mmol/L) reduced lipid droplet area and number; however, this effect was markedly attenuated following *RAB10* knockdown (Fig. S4F−S4I). These results indicate that BHB mitigates lipotoxicity and hepatic lipid accumulation in a RAB10-dependent manner.

3.6. BHB modulates RAB10−PLIN5 interaction to promote mitochondrial lipid droplet contacts

To understand how mitochondrial RAB10 facilitates lipid droplet-mitochondria interaction, we hypothesized that RAB10 may bind specific lipid droplet-associated proteins to mediate organelle communication. Immunofluorescence imaging of brown adipocytes transfected with mCherry-RAB10 and HIS-PLIN5 plasmids revealed co-localization of RAB10 and PLIN5 (Fig. 6A). This interaction was further confirmed through immunoprecipitation and molecular docking experiments, demonstrating that RAB10 interacts directly with PLIN5 (Fig. 6B−D). Molecular docking experiments revealed that the presence of BHB enhances the binding affinity of the RAB10−PLIN5 complex. The incorporation of BHB (10 mmol/L) significantly increased this interaction, a finding corroborated by immunoprecipitation experiments (Fig. 6E−G). These results suggest that BHB acts as a molecular modulator, strengthening the RAB10−PLIN5 interaction to promote organelle contact. *PLIN5* knockdown in brown adipocytes substantially attenuated the effect of BHB (10 mmol/L) in promoting MLC (Fig. 6H−J). Additionally, *PLIN5* knockdown inhibited maximal mitochondrial respiration, even in the presence of increased BHB levels (Fig. 6K and L, Fig. S4E). These results indicate that PLIN5 is critical for the functional role of RAB10 in mediating MLC, particularly under BHB modulation.

BHB mediates MLC in brown adipocytes by promoting the RAB10−PLIN5 interaction. This process enhances mitochondrial function and lipid droplet dynamics, highlighting a key molecular mechanism underlying BHB's regulatory role in brown adipose tissue metabolism.

3.7. BHB promotes mitochondria-lipid droplet contact in brown fat and reduces lipotoxicity in HFD-induced obese mice

Excessive fat accumulation leads to adipocyte hypertrophy, impaired mitochondrial oxidative metabolism, reduced lipid buffering capacity, and heightened inflammation, all of which contribute to MASLD[41,42]. Previous *in vitro* studies demonstrated that BHB promotes MLC in brown adipocytes *via* HADHA in hepatocytes. Notably, reduced HADHA expression and circulating BHB levels have been observed in MASLD model mice. To investigate the therapeutic effects of BHB, an obesity model was induced in C57BL/6J mice using a high-fat diet (HFD) for 12 weeks. Mice were then treated with BHB (100 mg/kg) through daily gavage for 20 days post-induction or weekly gavage for 8 weeks after 4 weeks of HFD induction (Fig. 7A). HFD-fed mice exhibited an increased number of lipid droplets in brown adipocytes and a reduction in MLD contact. BHB treatment significantly increased MLD contact area, decreased lipid droplet size, and restored mitochondrial cristae structure in brown fat (Fig. 7B−D). These findings mirrored *in vitro* observations. Histological analysis using HE staining revealed that HFD induced a transformation of brown fat from a "multicompartmental" to "unicompartmental" structure. BHB treatment restored the "multicompartmental" phenotype, enhancing thermogenic and metabolic capacity (Fig. 7E). In addition, BHB treatment markedly reduced the size and number of eWAT and iWAT (Fig. 7F−I). Oral glucose tolerance test (OGTT) and insulin tolerance test (ITT) results demonstrated that BHB alleviated HFD-induced insulin resistance (Fig. 7J and K).

In addition to metabolic improvements, BHB significantly reduced serum levels of non-esterified fatty acids (NEFA), triglycerides (TG), and total cholesterol (TC), all of which were negatively correlated with circulating BHB concentrations (Fig. 7L−P). Liver histological analysis further demonstrated that BHB treatment markedly ameliorated HFD-induced hepatic steatosis, hepatocyte ballooning, and lipid accumulation, as reflected by histological scoring and Doppler ultrasound measurements of liver lobe diameter (Fig. 7Q−S). Consistently, hepatic TC and TG levels were significantly reduced following BHB administration (Fig. 7T). Moreover, BHB restored hepatic FAO capacity, which was impaired by HFD feeding (Fig. 7U), and hepatic FAO showed a positive correlation with circulating BHB levels (Fig. 7V). qPCR analysis further demonstrated that BHB upregulated the expression of FAO-related genes, including *Cpt1a* and *Ppara* in the liver (Supporting Information Fig. S5A).

To evaluate the clinical relevance of these findings, plasma samples from patients with MASLD and healthy controls were analyzed. In line with the animal studies, MASLD patients exhibited significantly lower circulating BHB levels compared to healthy individuals (Fig. 7W).

Moreover, HFD-fed mice developed notable cardiac systolic dysfunction, including reduced EF% and FS% (Fig. S5B−S5D). BHB treatment significantly improved these cardiac parameters, restored the forward-to-reverse flow ratio, and normalized the aortic outflow tract internal diameter ratio (Fig. S5E−S5H).

Collectively, these findings indicate that BHB ameliorates obesity-related metabolic dysfunctions by enhancing adipose tissue function, promoting MLC formation in BAT, preventing adipocyte hypertrophy, facilitating lipid clearance, and alleviating hepatic lipotoxicity and cardiac dysfunction. Together, these multifaceted benefits underscore the therapeutic potential of BHB in treating obesity-associated MASLD and related metabolic disorders.

To further elucidate the role of hepatic HADHA in regulating BAT MLC formation under cold exposure, obesity was induced in mice *via* a 12-week HFD. Mice were then administered an adeno-associated virus serotype 8 (*AAV8*) vector encoding *HADHA* shRNA to specifically knock down hepatic *HADHA*. During a subsequent 20-day cold exposure period, mice received BHB treatment (100 mg/kg) (Supporting Information Fig. S6A). Efficient hepatic *HADHA* knockdown was confirmed (Fig. S6B and S6C).

Electron microscopy showed that HFD feeding reduced MLC formation in BAT, whereas cold exposure markedly enhanced

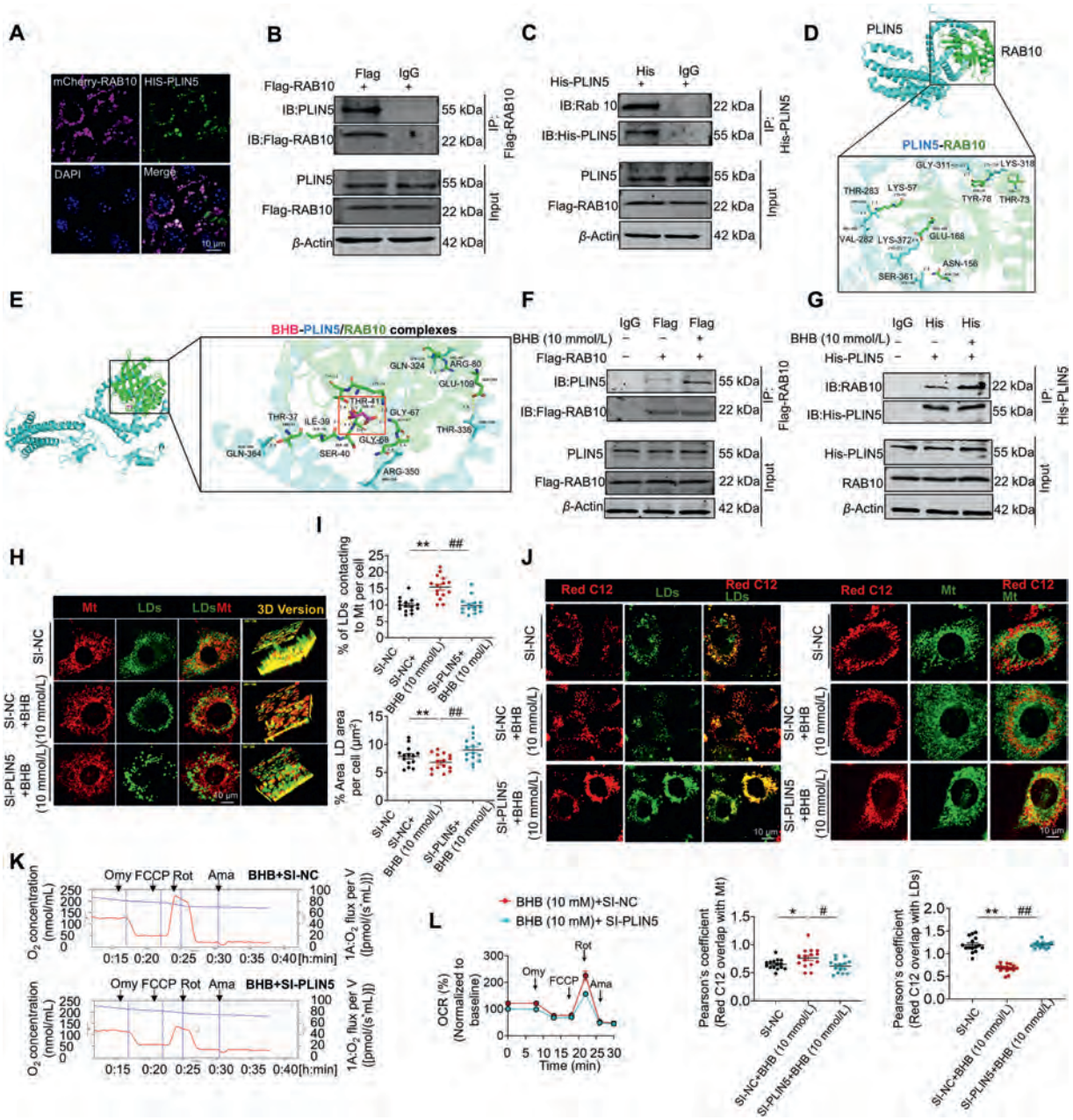

Figure 6 BHB modulates RAB10-PLIN5 interaction to promote mitochondrial lipid droplet contacts. (A) Co-localization of mCherry-RAB10 with HIS-PLIN5 in brown adipocytes detected by immunofluorescence. $n = 6$ in each group. (B) Brown adipocytes were transfected with Flag-RAB10. Immunoprecipitation (IP) was performed using anti-Flag antibody. IP assay showed that PLIN5 in brown adipocytes interacted with Flag-RAB10. $n = 3$ in each group. (C) Brown adipocytes were transfected with HIS-PLIN5. Immunoprecipitation (IP) was performed using anti-HIS antibody. IP assay showed that RAB10 in brown adipocytes interacted with HIS-PLIN5. $n = 3$ in each group. (D) Diagram of the molecular docking pattern of PLIN5 with RAB10. (E) Pattern of the molecular docking binding region of PLIN5 protein and RAB10−BHB complexes. (F, G) Immunoprecipitation to detect the effect of BHB on PLIN5 interaction with RAB10 in brown adipocytes. $n = 3$ in each group. (H, I) After knockdown of PLIN5 in brown adipocytes, changes in mitochondrial and lipid droplet effects of BHB on brown adipocytes were detected by Mitotracker and BODIPY staining. $n = 15$ in each group. (J) C12 and mitochondria were stained with Mitotracker Green or lipid droplets were stained with BODIPY. Statistics of FAs localization to mitochondria or FAs localization to LDs. $n = 15–16$ in each group. (K, L) Raw images and statistics of mitochondrial respiration assay in mature brown adipocytes. $n = 3$ in each group. Scale bar: 10 μm. Statistical analysis was performed with one-way ANOVA. $^{**}P < 0.01$ *vs.* NC, $^{\#\#}P < 0.01$ *vs.* SI-NC + BHB (10 mmol/L). Data are presented as mean ± SEM.

MLC. This enhancement was significantly attenuated in HADHA-deficient mice but rescued upon BHB supplementation (Fig. S6D−S6F). H&E staining of liver and adipose tissues revealed that cold exposure mitigated HFD-induced hepatic steatosis and lipotoxicity, effects that were blunted by hepatic *HADHA* knockdown but restored with BHB treatment (Fig. S6G−S6J). Consistently, circulating BHB levels increased following cold exposure (Fig. S6K).

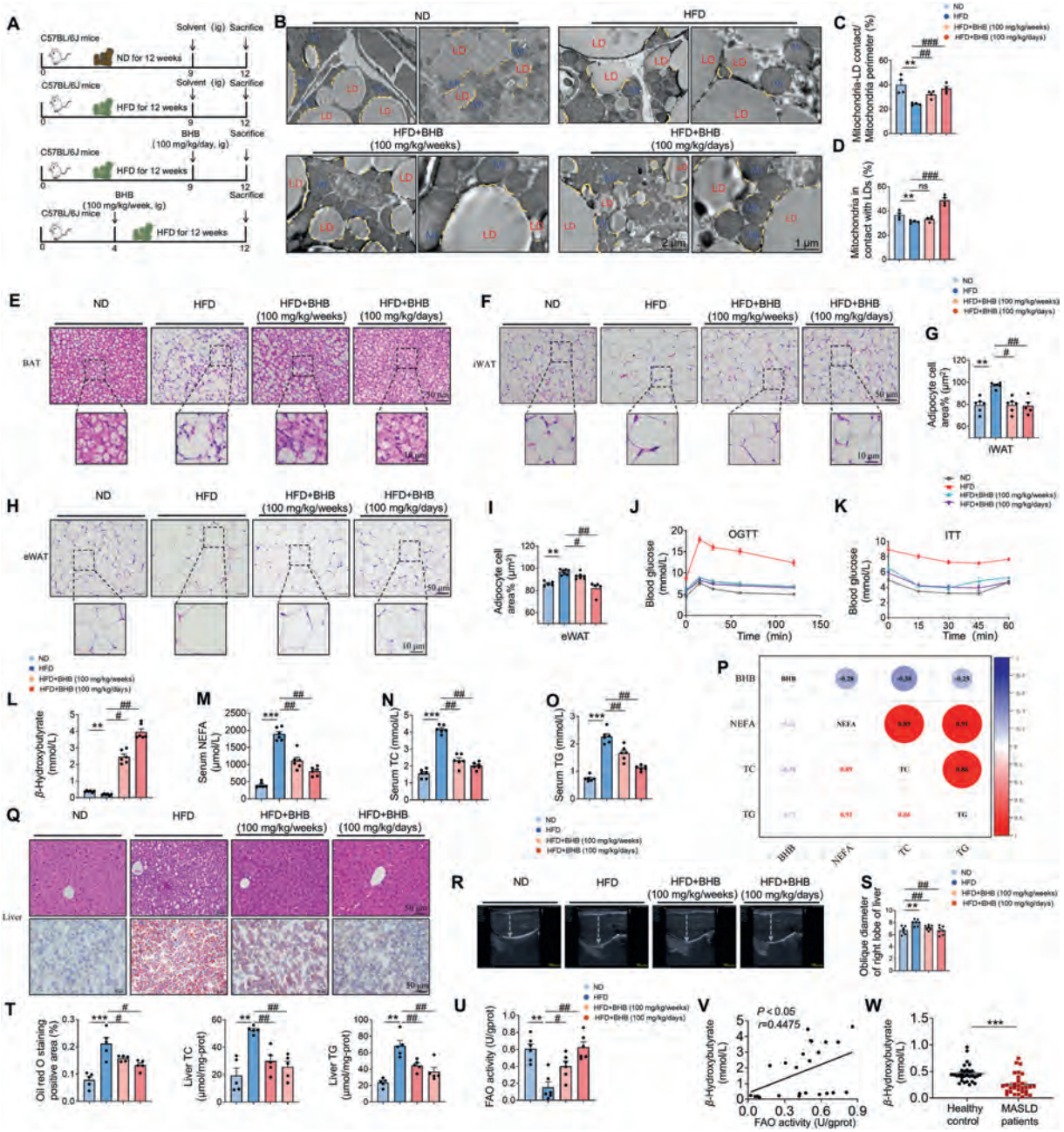

Figure 7 BHB promotes mitochondria-lipid droplet contact in brown fat and reduces lipotoxicity in HFD-induced obese mice. (A) Schematic illustration of the experiment design. (B−D) Electron microscopic observation of mitochondria and lipid droplets in brown adipose tissue of mice in each group, and on the mitochondria−lipid droplet contact area. And the number of mitochondria in contact with lipid droplets as a percentage of the total number of mitochondria was counted. $n = 3$ in each group. Scale bar: 1 or 2 cm. (E−I) Representative images of BAT, iWAT and eWAT biopsies stained with H&E and adipocyte area size statistics for iWAT, and eWAT. $n = 7$ in each group. (J, K) Insulin tolerance (ITT) and glucose tolerance tests (OGTT) were performed on all groups of mice. $n = 6$ in each group. (L) Statistics of BHB levels in mouse plasma. $n = 6$ in each group. (M, O) Statistics of free fatty acid (NEFAs), total Cholesterol (TC), and triglyceride (TG) content in mouse plasma. $n = 6$ in each group. (P) Correlation analysis of BHB content in mouse plasma with NEFA, TC and TG. $n = 24$ in each group. (Q, T) Representative images of live stained with H&E and Oil Red O. $n = 7$ in each group. Scale bar: 50 μm. (R, S) Representative Doppler ultrasound images of the liver and quantification of the oblique diameter of the right liver lobe. $n = 7$ in each group. (T) Hepatic TC and TG contents. $n = 5$ in each group. (U) Measurement of hepatic FAO capacity. $n = 5$ in each group. (V) Correlation analysis between hepatic FAO capacity and plasma BHB levels. $n = 20$ in each group. (W) Plasma asprosin levels in healthy controls and MASLD patients. $n = 30$ in each group. Statistical analysis was performed with one-way ANOVA. $^{**}P < 0.01$ *vs.* ND, $^{***}P < 0.001$ *vs.* ND, $^{\#}P < 0.05$ *vs.* HFD, $^{\#\#}P < 0.01$ *vs.* HFD. HFD, high-fat diet; ns, no significant. Data are presented as mean ± SEM.

Furthermore, liver Doppler ultrasound demonstrated improvements in hepatic lipid deposition and decreased oblique diameter of the right liver lobe upon cold exposure, both of which were diminished by hepatic *HADHA* knockdown but reversed by BHB administration (Fig. S6G−S6J).

These results demonstrate that hepatic HADHA−mediated BHB production facilitates MLC formation in BAT under cold exposure, thereby alleviating hepatic steatosis and lipotoxicity.

4. Discussion

The rapid improvement in human living standards has led to excessive nutrient and energy intake, driving a global surge in metabolic diseases. These conditions, including obesity, T2D, and MASLD, present substantial health challenges. A key pathological feature of these disorders is the ectopic lipid storage resulting from energy excess, which disrupts metabolic homeostasis[43-45]. Mitochondria play a central role in lipid metabolism by oxidizing FAs, thereby generating heat or ATP to support cellular activities. This makes the study of mitochondrial LD dynamics crucial for understanding lipid homeostasis and addressing metabolic diseases[15]. MLC, where LDs and mitochondria interact, enhance lipid transport efficiency and minimize lipid toxicity, making MLC regulation a critical research focus.

Brown and beige adipose tissue (BAT) are unique in their ability to dissipate chemical energy as heat through thermogenic respiration, offering promising therapeutic targets for metabolic disorders such as obesity and diabetes[46,47]. Cold exposure, a potent activator of BAT, enhances energy expenditure and improves metabolic profiles by activating β-adrenergic signaling[48]. However, the precise molecular mechanisms underlying these metabolic benefits remain incompletely understood. In this study, we identified a novel mechanism by which hepatic BHB drives MLC formation in BAT under cold exposure. Specifically, we discovered that BHB directly targets RAB10, a mitochondrial protein, through its interaction with the GLY-67 residue, as confirmed by SPIDER, pull-down, CETSA, DARTS, and molecular docking analyses. This interaction facilitates the formation of the RAB10−PLIN5 complex, which enhances MLC formation and promotes lipid utilization *via* mitochondrial oxidation.

The physiological significance of MLC across tissues has been a major focus in recent research. For instance, in tumor cells, hepatic phosphofructokinase phosphorylation enhances the PLIN2-CPT1A interaction to promote lipid mobilization[16]. Similarly, cardiomyocytes rely on mitochondrial protein MFN2 and LD protein HSC70 to mediate FAs transfer at MLC sites[17]. In skeletal muscle, RAB8A interacts with PLIN5 to regulate lipid metabolism in response to AMPK activation[24]. BAT-specific MLC dynamics have been less explored, despite recent discoveries of PeriDroplet Mitochondria, a subpopulation of mitochondria bound to LDs that play a critical role in lipid metabolism[49]. Our findings position RAB10 as a key mitochondrial regulator in BAT, interacting with PLIN5 to mediate MLC formation and lipid utilization under cold exposure.

PLIN5, an LD-associated protein, acts as a molecular switch for lipid metabolism by facilitating FAs transfer to mitochondria[50]. Previous studies have shown that PLIN5 interacts with FATP4 during nutrient deprivation to promote β-oxidation[19]. Small GTPases, such as Rab family proteins, are emerging as key regulators of intracellular trafficking and organelle interactions[51]. RAB8A, for instance, regulates MLC formation in skeletal muscle by interacting with PLIN5[24]. In BAT, our study highlights RAB10 as a novel BHB-responsive regulator that interacts with PLIN5 to form MLC, underscoring a critical pathway for efficient lipid utilization and thermogenic activation.

Traditionally, ketone bodies like BHB have been considered mere energy substrates produced during fasting or exercise[26,52]. However, accumulating evidence indicates that BHB also acts as a signaling molecule, modulating a variety of cellular and metabolic pathways. It has been shown to inhibit histone deacetylases, activate G protein−coupled receptors, promote liver regeneration, and reduce mitochondrial oxidative stress[53-56]. Emerging studies have linked BHB to novel pathways, such as BHB-amino acid generation, which regulates hypothalamic signaling and combats obesity[57]. Our findings expand this understanding by demonstrating that BHB enhances mitochondrial function, reduces lipotoxicity, and improves insulin sensitivity in HFD-induced obese mice. These multifaceted benefits position BHB as a promising therapeutic agent for metabolic diseases characterized by impaired BAT function and lipid dysregulation.

The liver plays a central role in systemic energy homeostasis and serves as the primary site for BHB synthesis *via* FAO[58]. Our study highlights the critical role of hepatic BHB in modulating MLC formation in BAT, with hepatic HADHA expression identified as a key regulatory factor. Conditioned media from hepatocytes overexpressing HADHA enhanced MLC formation in co-cultured BAT, characterized by smaller LDs, increased FAs trafficking from LDs to mitochondria, and improved mitochondrial FAO. In contrast, hepatic *HADHA* knockdown impaired these processes, which were restored upon BHB supplementation, thereby confirming the indispensable role of hepatic BHB in mediating inter-organ metabolic communication. Moreover, clinical data revealed significantly lower plasma BHB levels in MASLD patients compared to healthy controls, mirroring the reduction in hepatic FAO capacity observed in HFD-fed mice. Notably, circulating BHB levels positively correlated with hepatic FAO capacity, suggesting that BHB may serve as a potential diagnostic biomarker for MASLD. These findings underscore the importance of liver−BAT metabolic crosstalk in maintaining lipid and energy homeostasis, particularly under conditions of metabolic stress such as cold exposure.

Cold exposure activates the hypothalamus, triggering sympathetic nervous system stimulation and subsequent norepinephrine release[59,60]. NE-mediated β-adrenergic receptor activation upregulates key enzymes involved in ketogenesis, thereby elevating systemic BHB levels. Although BHB produced by BAT and other tissues under cold exposure contributes to MLC regulation within BAT, this quantitative contribution is likely limited due to tissue-specific metabolic capacities. The liver remains the primary source of circulating BHB and plays a dominant role in mediating its systemic metabolic benefits. Nonetheless, it is still important to further elucidate whether BHB produced by other tissues (including BAT) participates in the regulation of MLC or other metabolic processes.

5. Conclusions

This study establishes BHB as a pivotal mediator linking hepatic metabolism to BAT function. By promoting MLC formation *via* the RAB10−PLIN5 complex, BHB enhances mitochondrial efficiency and lipid utilization, offering a novel therapeutic avenue for addressing obesity, MASLD, and related metabolic disorders. Our

findings highlight the importance of inter-organ communication in metabolic regulation and suggest potential strategies to leverage these pathways in combating metabolic diseases.

Limitations of the study While this study provides important insights into the mechanistic role of BHB in regulating MLC in mouse BAT, its translatability to human BAT remains uncertain. Human BAT exhibits significant differences from mouse models in metabolic activity, thermogenic capacity, and anatomical distribution, which may limit the clinical applicability of these findings. Furthermore, our study predominantly focuses on hepatic BHB and BAT, without fully exploring the roles of other metabolically active organs, such as skeletal muscle or the central nervous system, in the systemic effects of cold exposure. Future studies investigating these broader inter-organ interactions and their contribution to cold-induced metabolic adaptations are essential to fully elucidate the therapeutic potential of BHB.

Acknowledgments

This work was supported by the Noncommunicable Chronic Diseases-National Science and Technology Major Project (2024ZD0537900, China), the National Natural Science Foundation of China (82170431, 82330011, and U21A20339), the CAMS Innovation Fund for Medical Sciences (CIFMS, 2020-I2M-5-003, China). We would also like to thank all the participants in this study for their tireless efforts.

Author contributions

Yuanyuan Yu: Investigation, Methodology, Writing original draft. Na An and Yi Chen: Conceptualization, Writing original draft. Ming Tong, Shuyu Liu, Yanrong Li and Hongbo Dong: Data curation, Visualization. Yanxi Li, Min Feng, Linhe Liu and Shifeng Cao: Data curation, Visualization. Huan Chen and Yixiu Zhao: Conceptualization. Zhimin Du: Visualization. Xin Zhao: Data curation, Visualization, Supervision. Baofeng Yang: Project administration, Supervision, Funding acquisition. Yan Zhang: Conceptualization, Funding acquisition, Writing review & editing.

Conflicts of interest

The authors disclose no conflicts of interest.

Appendix A. Supporting information

Supporting Information to this article can be found online at https://doi.org/10.1016/j.apsb.2025.11.014.

References

1. Swinburn BA, Kraak VI, Allender S, Atkins VJ, Baker PI, Bogard JR, et al. The global syndemic of obesity, undernutrition, and climate change: the lancet commission report. *Lancet* 2019;**393**:791−846.
2. Piche ME, Tchernof A, Despres JP. Obesity phenotypes, diabetes, and cardiovascular diseases. *Circ Res* 2020;**126**:1477−500.
3. Gilani A, Stoll L, Homan EA, Lo JC. Adipose signals regulating distal organ health and disease. *Diabetes* 2024;**73**:169−77.
4. Oikonomou EK, Antoniades C. The role of adipose tissue in cardiovascular health and disease. *Nat Rev Cardiol* 2019;**16**:83−99.
5. Bornstein MR, Neinast MD, Zeng X, Chu Q, Axsom J, Thorsheim C, et al. Comprehensive quantification of metabolic flux during acute cold stress in mice. *Cell Metab* 2023;**35**:2077-92.e2076.
6. Cannon B, Nedergaard J. Brown adipose tissue: function and physiological significance. *Physiol Rev* 2004;**84**:277−359.
7. Mills EL, Pierce KA, Jedrychowski MP, Garrity R, Winther S, Vidoni S, et al. Accumulation of succinate controls activation of adipose tissue thermogenesis. *Nature* 2018;**560**:102−6.
8. Gallardo-Montejano VI, Yang C, Hahner L, McAfee JL, Johnson JA, Holland WL, et al. Perilipin 5 links mitochondrial uncoupled respiration in brown fat to healthy white fat remodeling and systemic glucose tolerance. *Nat Commun* 2021;**12**:3320.
9. Hanssen MJ, Hoeks J, Brans B, van der Lans AA, Schaart G, van den Driessche JJ, et al. Short-term cold acclimation improves insulin sensitivity in patients with type 2 diabetes mellitus. *Nat Med* 2015;**21**:863−5.
10. Xiao F, Jiang H, Li Z, Jiang X, Chen S, Niu Y, et al. Reduced hepatic bradykinin degradation accounts for cold-induced BAT thermogenesis and WAT browning in male mice. *Nat Commun* 2023;**14**:2523.
11. Xu J, Cui L, Wang J, Zheng S, Zhang H, Ke S, et al. Cold-activated brown fat-derived extracellular vesicle-miR-378a-3p stimulates hepatic gluconeogenesis in male mice. *Nat Commun* 2023;**14**:5480.
12. Lynes MD, Leiria LO, Lundh M, Bartelt A, Shamsi F, Huang TL, et al. The cold-induced lipokine 12,13-diHOME promotes fatty acid transport into brown adipose tissue. *Nat Med* 2017;**23**:631−7.
13. Lidell ME, Enerback S. Brown adipose tissue—A new role in humans?. *Nat Rev Endocrinol* 2010;**6**:319−25.
14. Liu J, Zhang C, Zhang B, Sheng Y, Xu W, Luo Y, et al. Comprehensive analysis of the characteristics and differences in adult and newborn brown adipose tissue (BAT): newborn BAT is a more active/dynamic BAT. *Cells* 2020;**9**:201.
15. Rakotonirina-Ricquebourg R, Costa V, Teixeira V. Hello from the other side: membrane contact of lipid droplets with other organelles and subsequent functional implications. *Prog Lipid Res* 2022;**85**:101141.
16. Meng Y, Guo D, Lin L, Zhao H, Xu W, Luo S, et al. Glycolytic enzyme PFKL governs lipolysis by promoting lipid droplet-mitochondria tethering to enhance beta-oxidation and tumor cell proliferation. *Nat Metab* 2024;**6**:1092−107.
17. Hu L, Tang D, Qi B, Guo D, Wang Y, Geng J, et al. Mfn2/Hsc70 complex mediates the formation of mitochondria-lipid droplets membrane contact and regulates myocardial lipid metabolism. *Adv Sci (Weinh)* 2024;**11**:e2307749.
18. Olzmann JA, Carvalho P. Dynamics and functions of lipid droplets. *Nat Rev Mol Cell Biol* 2019;**20**:137−55.
19. Miner GE, So CM, Edwards W, Ragusa JV, Wine JT, Wong Gutierrez D, et al. PLIN5 interacts with FATP4 at membrane contact sites to promote lipid droplet-to-mitochondria fatty acid transport. *Dev Cell* 2023;**58**:1250-65.e1256.
20. English AR, Voeltz GK. RAB10 GTPase regulates ER dynamics and morphology. *Nat Cell Biol* 2013;**15**:169−78.
21. Xu R, Wan M, Shi X, Ma S, Zhang L, Yi P, et al. A RAB10−ACAP1−Arf6 GTPases cascade modulates M4 muscarinic acetylcholine receptor trafficking and signaling. *Cell Mol Life Sci* 2023;**80**:87.
22. Kiral FR, Kohrs FE, Jin EJ, Hiesinger PR. Rab GTPases and membrane trafficking in neurodegeneration. *Curr Biol* 2018;**28**:R471−86.
23. Nguyen MK, Kim CY, Kim JM, Park BO, Lee S, Park H, et al. Optogenetic oligomerization of Rab GTPases regulates intracellular membrane trafficking. *Nat Chem Biol* 2016;**12**:431−6.
24. Ouyang Q, Chen Q, Ke S, Ding L, Yang X, Rong P, et al. RAB8A as a mitochondrial receptor for lipid droplets in skeletal muscle. *Dev Cell* 2023;**58**:289−305.e286.
25. Qin C, Gong S, Liang T, Zhang Z, Thomas J, Deng J, et al. HADHA regulates respiratory complex assembly and couples FAO and OXPHOS. *Adv Sci (Weinh)* 2024;**11**:e2405147.

26. Pan A, Sun XM, Huang FQ, Liu JF, Cai YY, Wu X, et al. The mitochondrial beta-oxidation enzyme HADHA restrains hepatic glucagon response by promoting beta-hydroxybutyrate production. *Nat Commun* 2022;**13**:386.
27. Mendoza A, Takemoto Y, Cruzado KT, Masoud SS, Nagata A, Tantipanjaporn A, et al. Controlled lipid beta-oxidation and carnitine biosynthesis by a vitamin D metabolite. *Cell Chem Biol* 2022;**29**:660-9.e612.
28. Liu Y, Lu LL, Wen D, Liu DL, Dong LL, Gao DM, et al. MiR-612 regulates invadopodia of hepatocellular carcinoma by HADHA-mediated lipid reprogramming. *J Hematol Oncol* 2020;**13**:12.
29. Cai Z, Zhong Q, Feng Y, Wang Q, Zhang Z, Wei C, et al. Non-invasive mapping of brown adipose tissue activity with magnetic resonance imaging. *Nat Metab* 2024;**6**:1367−79.
30. Malloy VL, Perrone CE, Mattocks DA, Ables GP, Caliendo NS, Orentreich DS, et al. Methionine restriction prevents the progression of hepatic steatosis in leptin-deficient obese mice. *Metabolism* 2013;**62**:1651−61.
31. Gomora-Garcia JC, Montiel T, Huttenrauch M, Salcido-Gomez A, Garcia-Velazquez L, Ramiro-Cortes Y, et al. Effect of the ketone body, D-β-hydroxybutyrate, on sirtuin2-mediated regulation of mitochondrial quality control and the autophagy−lysosomal pathway. *Cells* 2023;**12**:486.
32. Newman JC, Verdin E. β-Hydroxybutyrate: a signaling metabolite. *Annu Rev Nutr* 2017;**37**:51−76.
33. Tian M, Ge E, Dong B, Zuo Y, Zhao Y, Lin W. Intramolecular spirocyclization enables design of a single fluorescent probe for monitoring the interplay between mitochondria and lipid droplets. *Anal Chem* 2021;**93**:3602−10.
34. Fan H, Tan Y. Lipid droplet-nitochondria contacts in health and disease. *Int J Mol Sci* 2024;**25**:6878.
35. Crabtree A, Neikirk K, Pinette JA, Whiteside A, Shao B, Bedenbaugh J, et al. Quantitative assessment of morphological changes in lipid droplets and lipid-mito interactions with aging in brown adipose. *J Cell Physiol* 2024;**239**:e31340.
36. Shi Y, Huang X, Zeng Y, Zhai M, Yao H, Liu C, et al. Endothelial TET2 regulates the white adipose browning and metabolism *via* fatty acid oxidation in obesity. *Redox Biol* 2024;**69**:103013.
37. Zhong J, He X, Gao X, Liu Q, Zhao Y, Hong Y, et al. Hyodeoxycholic acid ameliorates nonalcoholic fatty liver disease by inhibiting RAN-mediated PPARα nucleus−cytoplasm shuttling. *Nat Commun* 2023;**14**:5451.
38. Bartelt A, Heeren J. Adipose tissue browning and metabolic health. *Nat Rev Endocrinol* 2014;**10**:24−36.
39. Martinez TF, Lyons-Abbott S, Bookout AL, De Souza EV, Donaldson C, Vaughan JM, et al. Profiling mouse brown and white adipocytes to identify metabolically relevant small ORFs and functional microproteins. *Cell Metab* 2023;**35**:166-83.e111.
40. Chouchani ET, Kazak L, Jedrychowski MP, Lu GZ, Erickson BK, Szpyt J, et al. Mitochondrial ROS regulate thermogenic energy expenditure and sulfenylation of UCP1. *Nature* 2016;**532**:112−6.
41. Bansal SK, Bansal MB. Pathogenesis of MASLD and MASH—Role of insulin resistance and lipotoxicity. *Aliment Pharmacol Ther* 2024;**59**:S10−22.
42. Singh R, Barrios A, Dirakvand G, Pervin S. Human brown adipose tissue and metabolic health: potential for therapeutic avenues. *Cells* 2021;**10**:3030.
43. Okla M, Kim J, Koehler K, Chung S. Dietary factors promoting brown and beige fat development and thermogenesis. *Adv Nutr* 2017;**8**:473−83.
44. Liu J, Wang Y, Lin L. Small molecules for fat combustion: targeting obesity. *Acta Pharm Sin B* 2019;**9**:220−36.
45. Becher T, Palanisamy S, Kramer DJ, Eljalby M, Marx SJ, Wibmer AG, et al. Brown adipose tissue is associated with cardiometabolic health. *Nat Med* 2021;**27**:58−65.
46. Okamatsu-Ogura Y, Kuroda M, Tsutsumi R, Tsubota A, Saito M, Kimura K, et al. UCP1-dependent and UCP1-independent metabolic changes induced by acute cold exposure in brown adipose tissue of mice. *Metabolism* 2020;**113**:154396.
47. Sellers AJ, van Bee SMM, Hashim D, Baak R, Pallubinsky H, Moonen-Kornips E, et al. Cold acclimation with shivering improves metabolic health in adults with overweight or obesity. *Nat Metab* 2024;**6**:2246−53.
48. Yau WW, Yen PM. Thermogenesis in adipose tissue activated by thyroid hormone. *Int J Mol Sci* 2020;**21**:3020.
49. Benador IY, Veliova M, Liesa M, Shirihai OS. Mitochondria bound to lipid droplets: where mitochondrial dynamics regulate lipid storage and utilization. *Cell Metab* 2019;**29**:827−35.
50. Najt CP, Khan SA, Heden TD, Witthuhn BA, Perez M, Heier JL, et al. Lipid droplet-derived monounsaturated fatty acids traffic *via* PLIN5 to allosterically activate SIRT1. *Mol Cell* 2020;**77**:810-24.e818.
51. Morstein J, Bowcut V, Fernando M, Yang Y, Zhu L, Jenkins ML, et al. Targeting Ras-, Rho-, and Rab-family GTPases *via* a conserved cryptic pocket. *Cell* 2024;**187**:6379-92.e6317.
52. Wu Y, Teng Y, Zhang C, Pan Y, Zhang Q, Zhu X, et al. The ketone body beta-hydroxybutyrate alleviates CoCrMo alloy particles induced osteolysis by regulating NLRP3 inflammasome and osteoclast differentiation. *J Nanobiotechnol* 2022;**20**:120.
53. Lan Z, Chen A, Li L, Ye Y, Liang Q, Dong Q, et al. Downregulation of HDAC9 by the ketone metabolite β-hydroxybutyrate suppresses vascular calcification. *J Pathol* 2022;**258**:213−26.
54. Youm YH, Nguyen KY, Grant RW, Goldberg EL, Bodogai M, Kim D, et al. The ketone metabolite β-hydroxybutyrate blocks NLRP3 inflammasome-mediated inflammatory disease. *Nat Med* 2015;**21**:263−9.
55. Shippy DC, Wilhelm C, Viharkumar PA, Raife TJ, Ulland TK. β-Hydroxybutyrate inhibits inflammasome activation to attenuate Alzheimer's disease pathology. *J Neuroinflammation* 2020;**17**:280.
56. Guo M, Jiang X, Ouyang H, Zhang X, Zhang S, Wang P, et al. Parabacteroides distasonis promotes liver regeneration by increasing β-hydroxybutyric acid (BHB) production and BHB-driven STAT3 signals. *Acta Pharm Sin B* 2025;**15**:1430−46.
57. Moya-Garzon MD, Wang M, Li VL, Lyu X, Wei W, Tung AS, et al. A β-hydroxybutyrate shunt pathway generates anti-obesity ketone metabolites. *Cell* 2025;**188**:175-86.e120.
58. Cotter DG, Ercal B, d'Avignon DA, Dietzen DJ, Crawford PA. Impairments of hepatic gluconeogenesis and ketogenesis in PPARα-deficient neonatal mice. *Am J Physiol Endocrinol Metab* 2014;**307**:E176−85.
59. Lyons CE, Razzoli M, Larson E, Svedberg D, Frontini A, Cinti S, et al. Optogenetic-induced sympathetic neuromodulation of brown adipose tissue thermogenesis. *FASEB J* 2020;**34**:2765−73.
60. Tao X, Chen C, Chen Y, Zhang L, Hu J, Yu H, et al. β2-Adrenergic receptor promotes liver regeneration partially through crosstalk with c-met. *Cell Death Dis* 2022;**13**:571.
61. Jjiang HW, Chen H, Zheng YX, Wang XN, Meng Q, Xie J, et al. Specific pupylation as IDEntity reporter (SPIDER) for the identification of protein-biomolecule interactions. *Sci Chi Life Sci* 2023;**66**:1869−87.